Reaction Chemistry & Engineering

ROYAL SOCIETY OF CHEMISTRY

PAPER

View Article Online
View Journal

Cite this: DOI: 10.1039/d6re00061d

Structures of complexes formed by organophosphorus acid extractants and divalent metal ions

Stijn Raiguel, * Femke Derison and Koen Binnemans

The structure of metal–extractant complexes was investigated for Mg(II), Ca(II), Mn(II), Ni(II), Cu(II) and Zn(II) after solvent extraction by bis(2-ethylhexyl)phosphoric acid (D2EHPA) and bis(2,4,4-trimethylpentylphosphinic acid) (Ionquest® 290). A combination of slope analysis, Karl Fischer titration and differential scanning calorimetry (DSC) allowed the determination of the stoichiometry of the complex (both inner and outer sphere). UV-vis-NIR absorption spectroscopy was used to establish the coordination geometry and symmetry around the central metal ion, while infrared spectroscopy and ^{31}P NMR spectroscopy revealed structural characteristics of the extractant molecules and their coordination to the metal ion. Co(II), for which the structure is well-established in the literature, was used as a reference for infrared spectroscopy. The results indicate that all metals form oligomeric or polymeric structures at high loading, either as inner-sphere coordination polymers or as outer-sphere inverse micelles in the case of Ni(II). At lower loading, structures are more diverse, with the eventual structure of the complex being influenced by factors such as ionic radius, crystal field effects, steric demands of the extractant and the Jahn–Teller effect.

Received 20th February 2026,
Accepted 1st May 2026

DOI: 10.1039/d6re00061d

rsc.li/reaction-engineering

Introduction

Solvent extraction (SX) has been used on an industrial scale for the purification of metals since 1942, after its development was spurred by the need for high-purity uranium for the Manhattan project.[1] The utility of organophosphoric acids as extractants was serendipitously revealed in the early stages of SX research, as the hydrolysis products of organophosphate tri-esters were found to exhibit a higher affinity for uranium than the parent products under certain conditions.[2] This led to the introduction of bis(2-ethylhexyl)phosphoric acid (D2EHPA) in an industrial setting in 1955. The applications of this versatile and cost-effective extractant have since expanded to include zinc refining, cobalt production and rare-earth separations.[3,4] Other organophosphorus acids have joined D2EHPA on the market, including 2-ethylhexyl 2-ethylhexylphosphonic acid (EHEHP, marketed as PC-88A, Ionquest® 801 or P507) and bis(2,4,4-trimethylpentyl)phosphinic acid (marketed as Cyanex® 272 or Ionquest® 290). Recent research interest on these extractants has largely centered around recycling of critical metals, waste processing and process optimization.[5,6]

In spite of the abundance of research on the applications of D2EHPA, clear insights into the mechanism and selectivity of the extractant remain lacking. The gross reaction of the extraction process is often represented as follows:

$$M^{n+} + n\,\overline{HA} \rightleftharpoons \overline{MA_n} + n\,H^{+} \quad (1)$$

In eqn (1), M^{n+} denotes an n-valent metal ion, while HA represents the acidic form of the extractant, with A^- being its conjugate base. Overbars denote species in the organic phase. Thus, the extractant exchanges its acidic protons for positively charged metal ions from the aqueous phase such that the charge neutrality of both phases is respected. A complex is formed between the conjugate base of the extractant and the metal ion, stabilizing the cation in the apolar organic phase. The experimental order of selectivity of D2EHPA for metal ions is:[7]

$$Fe(III) > Zn(II) > Ca(II) > Mn(II) > Cu(II) > Mg(II) > Co(II) > Ni(II)$$

By contrast, Cyanex 272 and Ionquest 290 exhibit the following sequence:[7]

$$Fe(III) > Zn(II) > Cu(II) > Mn(II) > Co(II) > Mg(II) > Ca(II) > Ni(II)$$

The preference of both extractants for trivalent iron can be rationalized in terms of the increased electrostatic interaction between the higher-valent iron cation and the extractant anion. However, the origin of the sequence of other metals is not self-evident, nor is the difference in selectivity between

Department of Chemistry, KU Leuven, Celestijnenlaan 200F, P.O. box 2404, B-3001 Leuven, Belgium. E-mail: Stijn.Raiguel@kuleuven.be

the phosphoric and the phosphinic acids. Neither sequence corresponds to the well-known Irving–Williams series, which considers charge density and the Jahn–Teller effect of Cu(II) to postulate the following order of stability for coordination complexes of divalent fourth-period metal complexes: Mn(II) < Co(II) < Ni(II) < Cu(II) > Zn(II).[8,9]

Several studies have revealed that eqn (1) presents an oversimplified view of the extraction process and that the organic phase speciation is a function of the fraction of extractant molecules that have been deprotonated by loading with metal ions (*vide infra*), referred to as the percentage loading (%*L*):

$$\%L = \frac{[\overline{A^-}]}{c_{HA}} \cdot 100\% \quad (2)$$

In eqn (2), $[A^-]$ represents the equilibrium concentration of the deprotonated extractant, while c_{HA} denotes the analytical (*i.e.* initial) concentration of the extractant.

The speciation is further known to differ for various metal ions. Many authors have used slope analysis to prove that more than 2 extractant molecules are involved in complex formation at low loading. Slope analysis involves studying the dependence of the distribution of a metal as a function of the equilibrium concentration of one of the species partaking in the reaction in order to determine the stoichiometric coefficient of this species. It can be shown (see the SI, page S3) that the logarithm of the distribution ratio (*D*) varies linearly with the logarithm of the equilibrium concentration of the extractant at constant pH, with the slope corresponding to the number of extractant dimers $(HA)_2$ involved in the gross reaction corresponding to the extraction of one metal ion. *D* is defined as the ratio of the organic concentration of a metal ion to its aqueous concentration:

$$D = \frac{[M^{n+}]_{org}}{[M^{n+}]_{aq}} \quad (3)$$

with subscripts aq and org denoting the aqueous and organic phase, respectively. A number of assumptions are made, including (1) the absence of ionic strength effects, (2) immiscibility of the phases, (3) the invariability of the extraction mechanism as a function of the concentrations and (4) full dimerization of the extractant. The latter is a reasonable assumption for organophosphorus acid extractants diluted in aliphatic diluents.[10–12] In an alternative formulation, the quantity log(*D*) − 2pH can be plotted against the logarithm of the equilibrium extractant concentration to obtain the same theoretical slope, obviating the need for pH control.

Slope analysis has indicated that fourth-period divalent metal ions, such as Mn(II), Co(II), Cu(II) and Zn(II), usually bind to two extractant dimers upon extraction by organophosphorus acid extractants, *i.e.* four extractant molecules, up to a loading of 50%.[11–17] Ni(II) has even been proven to bind to three dimers in order to fulfill its preference for six-coordinate structures.[13,18] These results are incompatible with eqn (2). Furthermore, it is evident that the aforementioned complexes cannot exist at 100% loading of the extractant on stoichiometric grounds. At 100% loading, the extractant must be fully deprotonated and present in a 2 : 1 ratio with respect to the extracted metal ion. Instead, results obtained by earlier authors strongly suggest the formation of larger structures under these conditions, evidenced by vapor pressure osmometry, an increase in viscosity of the solutions for several metals, large hydrodynamic radii as obtained by dynamic light scattering (DLS), and an increase in the apparent equilibrium constant of the extraction process at higher loading.[13,20–25] The nature of these aggregates is not yet fully understood, and both supramolecular aggregation and the formation of coordination polymers has been proposed.[20,22] For some metals, such as Ni(II), coextraction of stoichiometric amounts of water also appears to be an integral part of the extraction mechanism, another phenomenon not predicted by eqn (2).[20,26] Differences in extraction behavior of the various phosphorus acid extractants are often explained in terms of the formation of analogous coordination complexes with slight variations in properties, notwithstanding the lack of evidence to support the assumption that the formed structures are necessarily analogous.[27–29]

In this work, the structures of the metal complexes of Mg(II), Ca(II), Mn(II), Co(II), Ni(II), Cu(II) and Zn(II), formed after extraction by D2EHPA and Ionquest 290 in an aliphatic diluent, were studied using various instrumental and titrimetric techniques. Samples were studied at low, medium and high loading and the results are discussed in light of the preexisting literature. This study focuses on extraction from sulfate solutions, as chloride anions are known to incorporate in the extracted complex for some transition metal ions with a strong propensity for chloride coordination.[30]

Experimental

Chemicals and reagents

Cobalt(II) sulfate heptahydrate (99+%), zinc(II) sulfate monohydrate (99%), sodium hydrogen carbonate (analytical reagent grade), calcium hydroxide (98+%) and molecular sieves (3 Å) were purchased from Acros Organics (Geel, Belgium). Copper(II) sulfate pentahydrate (≥98%) and 1-butanol (≥99.4%) were procured from Merck nv (Overijse, Belgium). Manganese(II) sulfate monohydrate (a.r.), magnesium chloride hexahydrate (v.p.) and methanesulfonic acid 0.4 mol L^{-1} (cation eluent concentrate) were obtained from Chem-Lab nv (Zedelgem, Belgium). Sodium hydroxide (pearl, analytical reagent grade), bis(2-ethylhexyl)phosphoric acid (95%) and heptane fraction from petroleum (laboratory reagent grade) were purchased from Thermo Fisher Scientific BV (Merelbeke, Belgium). 1-Butyl-3-methylimidazolium bromide (99%) was obtained from IoLiTec – Ionic Liquids Technologies GmbH. Nickel(II) sulfate hexahydrate (p.a.) was purchased from Th. Geyer GmbH (Renningen, Germany). Exxsol D120 was procured from ExxonMobil Petroleum &

Chemical (Machelen, Belgium). Ionquest 290 was purchased from Italmatch Chemicals (Genova, Italy). Molecular sieves were activated by drying overnight at 120 °C and a pressure of 1 mbar. All other chemicals were used as received. Water used for analysis was always of ultrapure quality, purified to a TOC of <2 ppb and deionized to a resistivity of 18.2 MΩ cm by a Millipore Milli-Q Reference® system.

Impurities in bis(2-ethylhexyl)phosphoric acid (D2EHPA) and Ionquest 290 were assessed using ^{31}P NMR. Small concentrations of 2-ethylhexylphosphoric acid and inorganic phosphates were found in D2EHPA, while traces of phosphinic acids with other side chains are present in Ionquest 290. The concentrations hereof are sufficiently low (≤2 mol%) to not significantly affect the analyses carried out in this work.

Instrumentation

Concentrations of magnesium and calcium in aqueous samples were determined by ion chromatography on a Shimadzu device consisting of a CBM-40 system controller, DGU-403 degassing unit, LC-20Ai pump, SIL20A autosampler, CTO-40C column oven and CDD-10A vp conductivity detector. A Shodex YS-40 column was used. The eluent consisted of 4 mM methanesulfonic acid in ultrapure water. The oven temperature was set at 40 °C and the flow rate of the eluent was 1.0 mL min^{-1}. Samples were diluted to obtain concentrations in the 1–200 ppm range for every analyte. The injection volume was varied between 3 and 10 μL in order to obtain both sufficient peak intensity and resolution. Calibration was performed using an external standard solution series, to which a linear calibration curve was fitted.

High-field nuclear magnetic resonance (NMR) spectra were recorded on a Bruker Avance Neo 600 spectrometer with an Ascend™ 600 magnet system and a 5 mm PI HR-TBO (BB/F-H/F-D) probe with *z*-gradients. Data were recorded at room temperature (22 °C) using Bruker TopSpin 4 and processed and analyzed using Spinworks 4.2.12. Data were calibrated using the phosphorus signal obtained from 10 vol% H_3PO_4 in D_2O in a glass capillary insert. Moisture-sensitive samples were recorded in sample tubes fitted with a glass screwcap, sealed with PTFE tape and flushed with dry nitrogen gas. The chemical shift (δ) values are expressed in parts per million (ppm).

Infrared spectra were measured in attenuated total reflectance (ATR) mode on a Bruker Vertex 70 infrared spectrometer equipped with RAMII Raman module, diamond sample crystal and a 1064 nm laser source. Spectra and background were recorded in 32 scans between 400 and 4000 cm^{-1} at a resolution of 2 cm^{-1} and processed using the OPUS software package. UV-vis-NIR spectra were recorded between 350 and 1350 nm on an Agilent Cary 6000i spectrophotometer at a resolution of 1 nm and processed using the Cary WinUV software package. Differential scanning calorimetry (DSC) was performed on a METTLER TOLEDO DSC822e instrument at a scan rate of 2 °C min^{-1}. A sample of approximately 15 mg was used in a pierced 40 μL Al pan under a He atmosphere (30 mL min^{-1}). Densities were measured using an Anton Paar Lovis 2000 M/ME densitometer/viscometer. pH measurements were carried out on a METTLER TOLEDO SevenCompact pH meter in combination with a Mettler–Toledo InLab Micro glass electrode.

Karl Fischer titration was carried out using either a METTLER TOLEDO V30S volumetric titrator or a C30S coulometric titrator. The latter was used for samples with very low concentrations of water and those containing Cu(II), as the potentiometric end point detection method used by the volumetric titrator is incompatible with the presence of Cu(II). While Cu(II) may act as an interferent in Karl Fischer titrations due to its oxidizing nature, reduction of Cu(II) to the insoluble, colorless copper(I) iodide was not observed.

Preparation of loaded samples

Samples of loaded extractants for spectroscopic studies were prepared by loading a solution (2–5 mL) of the extractant in heptane (mixture of isomers), unless otherwise stated. The organic phase was allowed to come in contact with an equal volume of an aqueous solution containing the necessary amount of NaOH in order to saponify (neutralize) the extractant to the desired loading. The aqueous phase further contained an excess (approx. 1 mol L^{-1}) of the desired transition metal ion as the sulfate salt (or chloride in the case of Mg(II)). The samples were then shaken overnight, and phase disengagement was subsequently expedited by centrifugation. The dissolution of the metal hydroxide precipitate was used as a visual cue for the attainment of equilibrium. For samples loaded with Ca(II), an alternative method was used in which a stoichiometric amount $Ca(OH)_2$ was suspended in the aqueous phase. Equilibration was carried out as above, with the dissolution of the hydroxide serving as an indication of the attainment of equilibrium.

Preparation of partially hydrated samples of Ni(II)-loaded extractants

In order to prepare samples of Ni(II) in D2EHPA and Ionquest 290 with a well-defined degree of hydration, anhydrous samples of the nickel salts of both extractants were first prepared. The Ni(II) salt of D2EHPA was prepared by first adding a solution of 12.50 g (38.8 mmol) in 100 mL heptane to an equal volume of $NaHCO_3$ solution. This initial step removes mono(2-ethylhexyl)phosphoric acid and inorganic phosphate impurities. Subsequently, the organic phase was stirred for 3 days with an equal volume of water containing 1.02 eq. (1.58 g, 39.5 mmol) of NaOH. An aqueous pH of 12 or lower indicates completion of the neutralization of D2EHPA by NaOH. After neutralization, the organic phase was stirred twice for 2 hours with 100 mL of a 0.195 mol L^{-1} solution of $NiSO_4$ (*i.e.* 0.503 eq. per step), where the disappearance of the green color of Ni(II) from the aqueous phase signals the achievement of full exchange of Na(I) for Ni(II). The organic phase was finally dried over 50 g of activated 3 Å molecular sieves (5 days), resulting in a color change from green to yellow-orange. After filtration, the

filtrate was evaporated to dryness under reduced pressure, yielding 9.96 g (14.2 mmol, 73%) of a yellowish brown solid.

The Ni(II) salt of Ionquest 290 was prepared by adding a solution of 20.00 g (68.9 mmol) of Ionquest 290 in 100 mL of heptane and 10 mL of 1-butanol to an equal volume of water containing 1.02 eq. (2.82 g, 70.5 mmol) of NaOH and 0.503 eq. (9.10 g, 34.6 mmol) of $NiSO_4$. The mixture was stirred overnight at 40 °C, with the dissolution of the $Ni(OH)_2$ precipitate indicating completion of the reaction. Subsequently, the organic phase was added to 100 mL of a 120 g L^{-1} solution of $NiSO_4$ and washed with 100 mL of water. The organic phase was finally dried over 40 g of activated 3 Å molecular sieves (5 days), resulting in a color change from green to brown. After filtration, the filtrate was evaporated to dryness under reduced pressure, yielding 9.96 g (30.0 mmol, 87%) of a blue solid.

The solids were redissolved in heptane to a concentration of 10 wt%, and appropriate amounts of water were added under an argon atmosphere in order to reach the desired degree of hydration. The concentration of water was verified by Karl Fischer titration. Anhydrous samples were dried a second time over activated 3 Å molecular sieves under an argon atmosphere for at least 4 days.

Slope analysis

Slope analysis was performed by preparing a series of biphasic samples in 20 mL vials with a volume of 5 mL per phase. The organic phase consisted of varying concentrations of the extractant (12–60 vol%), while the aqueous phase consisted of 0.15 mol L^{-1} $CaCl_2$ or $MgCl_2$ and 0.15 mol L^{-1} NaOH. The phases were equilibrated by shaking overnight, and phase disengagement was subsequently expedited by centrifugation. The dissolution of the hydroxide precipitate served as an indication of the attainment of equilibrium.

Results and discussion

Cobalt(II)

Cobalt(II) is the best-studied of the metal ions considered in this work, and is therefore discussed first and used as a reference for the other examples (in particular for FT-IR spectroscopy). Literature data were extended by our own experimental data. Brisk and McManamey determined the number of D2EHPA dimer molecules involved in the extraction process of Co(II) and found this number to be 2 at lower loading (<10%). However, above 50% loading, insufficient D2EHPA molecules are present to form the $Co(HA_2)_2$ structure. At a loading of 100%, the only possible stoichiometry is CoA_2. Loading beyond 50% concurrently results in a drastic increase in viscosity, which Brisk and McManamey attributed to the formation of polymeric structures.[22] The tetrahedral geometry of the cobalt ion in both the $Co(HA_2)_2$ and the CoA_2 structure are evident from the blue to violet color of the organic phase over the entire loading range and the presence of the corresponding absorption bands in UV-vis absorption spectra.[22,31]

Thiyagarajan *et al.* conducted neutron scattering studies on samples of phosphoric, phosphonic and phosphinic acid extractants loaded with Co(II), concluding that all three extractant types form polymers under high loading conditions.[32] For D2EHPA and purified Cyanex 272 (virtually identical in composition to Ionquest 290), these polymers had a high degree of polymerization and were cylindrical in nature. The authors found the polymer length to increase with loading and hypothesized that excess extractant induces chain termination by binding as a dimer in a manner similar to its coordination in the $Co(HA_2)_2$ monomers. The authors observed an increase in the apparent radius of the Cyanex 272 polymer with loading, which was interpreted as the formation of crosslinks between chains at very high loading. The degree of polymerization was more or less independent of the extractant concentration for the Cyanex 272 system, while the D2EHPA system exhibited an increase in chain length with increasing extractant concentration. Overall, the authors concluded the structure of the metal–extractant complex to be a coordination polymer at high loading conditions, with Co(II) centers linked by bridging extractant anions. The authors noted that the structure could consist of either a polymer in which every pair of Co(II) centers is linked by two bridging extractant anions or one in which single and triple bridges alternate (Fig. 1, structure type II and III).

Neuman and coworkers extensively analyzed the structures formed by D2EHPA at 100% loading as well and postulated an alternative micelle-type structure in which tetrahedral CoA_2 units aggregate through weak intermolecular interactions.[27,31] Unlike Thiyagarajan *et al.*, these authors noted a decrease in the aggregation number with increasing CoA_2 concentration, as determined by vapor pressure osmometry. The authors interpret this result as evidence that the aggregates are highly dynamic in nature and governed by the type of intermolecular interactions that are pertinent in solutions of surfactants, where higher concentrations are often observed to yield smaller aggregates. However, it should be noted that even coordination polymers in solution can be dynamic, in particular as the ligand exchange kinetics of the Co(II)–extractant systems are relatively rapid.

Best and coworkers reported that EXAFS results support the coordination polymer hypothesis, at least for Cyanex 272.[33] The authors compared Co–ligand and Co–Co distances determined by EXAFS of the loaded organic phase with those obtained by XRD of crystallized cobalt(II) organophosphinate structures. The distances accorded well and were consistent with a covalent framework rather than weakly interacting mononuclear complexes. In fact, the structure elucidation yielded a result in remarkable agreement with a coordination polymer consisting of two bridging phosphinate ligands per pair of adjacent Co(II) centers (Cambridge Structural Database identifier JIRNON), far more so than a structure with alternating single and triple bridges (Cambridge Structural Database identifier WACROH).

Further support for these structures (in Cyanex 272) was provided by Carson and coworkers in the form of ^{31}P NMR

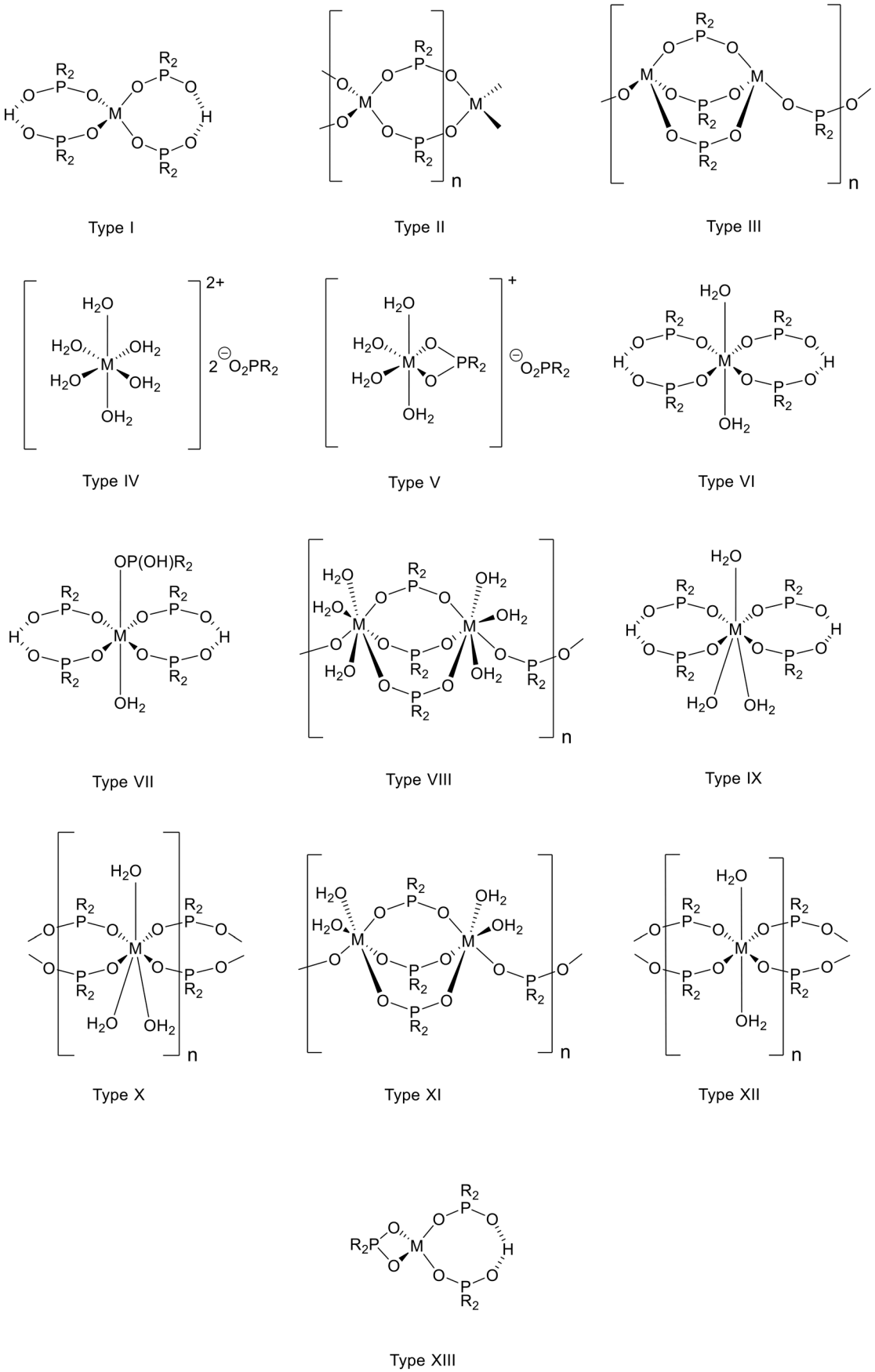

Fig. 1 Overview of structures observed in the organic phase after extraction of divalent metal ions by D2EHPA and Ionquest 290.

spectroscopy and *ab initio* calculations.[25] It was found that all free $(HA)_2$ was consumed in the vicinity of 50% loading, supporting a $Co(HA_2)_2$ stoichiometry. Calculations using density functional theory (DFT) showed that CoA_2 spontaneously polymerizes, while the reaction between CoA_2 and $(HA)_2$ favors the formation of $Co(HA_2)_2$. Large structures at high loading were also supported by diffusion-ordered NMR spectroscopy (DOSY). Unfortunately, the relative stability of the two polymeric structures considered by Best was not investigated, and a double-bridged structure was assumed.

The shift in speciation at higher loading can be rationalized in terms of a shift in equilibrium as the concentration of free extractant, $(HA)_2$, decreases. At all times, the low-loading and high-loading structures are in equilibrium as described by eqn (4):

$$n\,Co(HA_2)_2 \rightleftharpoons (CoA_2)_n + n(HA)_2 \quad (4)$$

As the amount of free extractant decreases, the equilibrium shifts towards the right, resulting in the formation of polymers. Brisk and McManamey envisioned this process as being stepwise, with $Co(HA_2)_2$ first reacting with Co(II) ions to form dimers and oligomers.[22] This hypothesis is based on measurements of viscosity as a function of loading, which indicate a progressive increase in degree of polymerizations in metal–D2EHPA systems.[21,22] Beyond 50% loading, it is no longer possible for all Co(II) to be present as $Co(HA_2)_2$ on stoichiometric grounds.

FT-IR spectra were recorded of the phosphorus–oxygen bond region of D2EHPA (245 g L^{-1}) and Ionquest 290 (183 g L^{-1}) in heptane after loading with Co(II) and are shown in Fig. 2. Spectra were recorded at a loading of 30%, 50% and 100%, corresponding to a 3 : 1, 2 : 1 or 1 : 1 stoichiometry of Co(II) and $(HA)_2$. However, only the spectra for 50% and 100% loading are shown below, as the spectral features of the extracted complex are identical at 30% and 50% loading (spectra for 30% loading shown in the SI, Fig. S1 and S2). Many of the spectral features of the phosphate/phosphinate symmetrical and antisymmetrical stretching bands correspond to aforementioned structures reported in the literature.

The D2EHPA spectrum at 50% loading exhibits a bathochromic shift of the antisymmetrical stretching band with respect to unloaded D2EHPA, from 1229 to 1197 cm^{-1}. In contrast, the symmetrical stretching band remains largely unshifted at 1031–1032 cm^{-1}. The asymmetry of this band is likely due to overlap with the P–OC stretching band. The bathochromic shift of the antisymmetrical component reflects the reduction in bond order in the phosphoryl group from 2 to 1.5 upon deprotonation. Furthermore, a reduction of the split of the antisymmetrical and symmetrical stretching bands is associated with an increase in symmetry of the local symmetry around the phosphoryloxy group.[34] This reduced splitting is clearly visible and can be attributed to the formation of HA_2^- ligands. In the D2EHPA $(HA)_2$ dimers, a clear distinction exists between the double and the

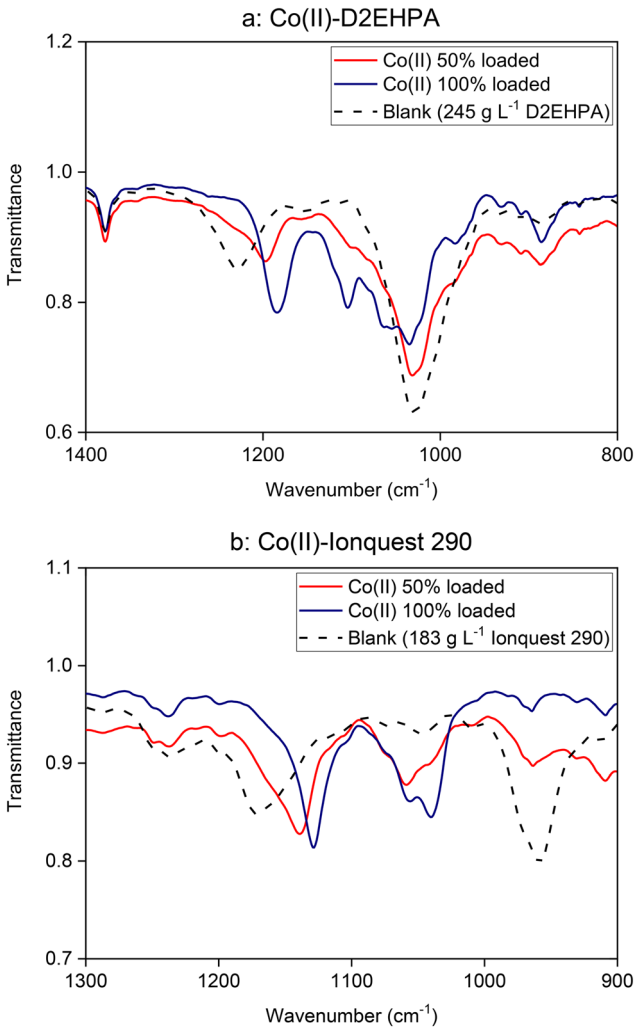

Fig. 2 FT-IR spectra of D2EHPA (245 g L^{-1} in heptane (a), and Ionquest 290 (183 g L^{-1} in heptane (b) after loading with cobalt(II). Peaks are listed in the SI (Table S1).

single phosphorus–oxygen bonds. Upon deprotonation, one might expect the emergence of two sets of bands, one corresponding to the protonated HA molecule and one corresponding to the symmetrical and antisymmetrical components of the A^- anion with bond order 1.5. However, XRD analysis of solid state organophosphoric acid dimers has indicated that protons are strongly shared between two phosphate moieties, which clarifies why infrared spectra show only a single set of bands for $(HA)_2^-$ dimers. The local symmetry around the phosphoryloxy is intermediate between a bidentate A^- anion and a protonated HA molecule.[35] The spectra thus appear consistent with structure type I (Fig. 1), which was also postulated by Brisk and McManamey.[22]

At a loading of 100%, the spectrum of the D2EHPA solution changes markedly (Fig. 2b). The gap between the symmetrical and antisymmetrical stretching bands further reduces, indicating an even higher degree of symmetry. This is consistent with the formation of bridging A^- anions, as hypothesized by Thiyagarajan, Carson and Best.[25,32,33] The

symmetrical component adopts a very complex splitting pattern. Two main subgroups appear to be present: one centered around 1104 cm^{-1} without further fine structure, and a second, more intense group with a barycenter at approx. 1049 cm^{-1}, consisting of three identifiable components. Such splitting can occur either due to coexistence of multiple distinct chemical environments for the phosphate group or due to intramolecular vibrational coupling of normal modes with one another. The latter phenomenon is especially prominent in the crystalline solids (in which case it is referred to as Davydov or factor group splitting), and selection rules are governed by group theoretical considerations.[36] The splitting of degenerate modes by the reduction of local symmetry (site group splitting) through complexation can be excluded, as the point group describing the phosphate group of the D2EHPA anion (C_{2v}) does not feature degenerate representations.[37] If the solution state structure of the polymer exhibits sufficient local ordering, a structure with two phosphate bridges per pair of Co(II) centers (Fig. 1, type II) could plausibly result in the emergence of up to two bands, depending on the local symmetry of the compound. However, crystals of transition metal organophosphates appear to generally adopt the alternating triple and single bridged polymeric structure (Fig. 1, type III).[38] Such a structure results in four non-identical phosphate environments: a group of three, each differing in their orientation relative to the fourth phosphate group, which connects the apices of two triple-bridged cobalt-phosphate clusters. This structure offers a satisfactory assignment of the bands seen in Fig. 2a, with the weaker band at 1104 cm^{-1} corresponding to the single bridge, and the intense group of three bands centered around 1049 cm^{-1} corresponding to the triple bridge. The smaller splitting of the symmetrical and antisymmetrical components in the single bridge and the inequivalence of the phosphate groups in the threefold bridge is similar to what is observed in analogous zinc carboxylate species.[39]

The spectrum of Ionquest 290 at 50% loading with Co(II) (Fig. 2b) exhibits a bathochromic shift of the barycenter of the phosphinate spectrum and a contraction of the gap between the symmetrical and the antisymmetrical components with respect to unloaded Ionquest 290, in a fashion similar to that of D2EHPA. The spectrum at 30% loading is omitted from Fig. 2b as it is qualitatively identical to that at 50% loading, suggesting no change in speciation. The symmetrical component appears split into a distinct peak at 1059 cm^{-1} and a shoulder at lower wavenumber. Analysis of the blank-subtracted spectrum and deconvolution (see the SI, Fig. S3 and S4) indicates that this shoulder is located at 1038 cm^{-1} and thus distinct from the overlapping background signal located at approximately 1047 cm^{-1}. This split can be rationalized in terms of dimer formation. Unlike D2EHPA, the acidity of phosphinic acids is limited, and the proton is shared to a lesser degree between the members of the HA_2^- dimer. This is indicated by computational studies as well as XRD structures.[40,41] Hence, the coordinating HA_2^- dimer can be expected to give rise to two distinct bands in the infrared spectrum, and the spectrum is consistent with structure I as shown in Fig. 1, as proposed by Brisk and McManamey for the Co(II)–D2EHPA complex at low loading.

At 100% loading with Co(II), a bathochromic shift of the antisymmetrical component further reduces the gap between the two phosphinate stretching components. This is indicative of the formation of highly symmetrical bridging phosphinate groups. Interestingly, the antisymmetrical component remains split into two bands of roughly equal intensity at 1055 and 1040 cm^{-1}. This split is frequently observed in crystals of transition metal phosphinate coordination polymers.[34,42–44] Nonetheless, examples of the contrary exist as well.[34,40,42] Oliver attributed this to the presence of crystallographically dissimilar phosphinate positions in the structure, with different metal-to-ligand bond distances.[42] The magnitude of the splitting also appears to be compatible with an equilibrium between tightly and loosely bound ligands observed in solid metal–organic framework structures.[45] Similar splitting has been observed in crystallized cobalt(II) diphenylphosphinate chains of both structural types (Fig. 1, type II and III) and its mere presence is thus not suitable as a diagnostic feature.[46,47] The difference in frequency between the symmetrical components of the two phosphinate groups in type II structures is thus similar to those of the triple *versus* the single bridges in type III, while the difference in frequency of the groups within the triple bridge are insufficiently dissimilar to be resolved. Nonetheless, the two bands in the Co(II)–Ionquest 290 solution (Fig. 2b) are approximately equal in integration, in contrast to those visible in the Co(II)–D2EHPA system, suggesting an equal number of phosphinate groups contribute to both bands in the Co(II)–Ionquest 290 spectrum (assuming the bonding to be sufficiently similar across various types of bridging phosphinate groups to result in similar oscillator strengths). Furthermore, the results obtained by Best *et al.* strongly support a structure with only double phosphinate bridges linking pairs of Co(II) centers (Fig. 1, type II), and spectra with this type of splitting will be considered to be compatible with polymers of this structural type in further discussion.

Nickel(II)

Nickel(II) has also received considerable research interest in the context of solvent extraction by D2EHPA. Several authors have subjected this system to slope analysis, revealing that at low loading of the extractant (<10%), Ni(II) is extracted into discrete, mononuclear complexes with stoichiometry NiH_4A_6 in aliphatic diluents, thus binding an additional $(HA)_2$ dimer as compared to Co(II).[26,48,49] This reflects the propensity of Ni(II) to form octahedral complexes as a result of the high ligand field stabilization energy in octahedral Ni(II) complexes with respect to their tetrahedral counterparts. In aromatic or polar diluents, Komasawa *et al.* found a 1:2

stoichiometry between Ni(II) and the D2EHPA dimer through slope analysis. This ratio indicates the substitution of one dimer in the first coordination sphere by either water molecules or polar diluent molecules, yielding a less lipophilic complex that can be stabilized by the more polar medium.[26] Under certain conditions, a 1 : 4 stoichiometry was reported by Preston, although it must be noted that slope analysis does not distinguish between inner- and outer-sphere coordination.[50] The results thus do not necessarily imply 8-fold coordination.

At higher loading conditions, which are more representative for industrial applications, an aggregate structure is known to occur in Ni(II)–D2EHPA systems. Neuman and coworkers identified large structures in solution using dynamic light scattering (DLS) measurements, similar to what was observed for other metal ions. The nickel(II) structures, however, were distinct in their ability to solubilize large amounts of water, up to 11 molecules per Ni(II) center.[51] Small-angle neutron scattering (SANS) revealed the structures to be cylindrical in nature, with a constant diameter.[52] The amount of water solubilized by these structures is too large to be accommodated in the inner sphere of the Ni(II) ions, suggesting a micellar structure (capable of interacting with water) as opposed to a coordination polymer, which would lack hydrophilic pockets. The presence of water affects the growth of the micelles as the aggregation number appears to be limited to about 5 under dry or partially hydrated conditions, but full hydration allows the formation of large aggregates at high concentrations of Ni(II)-loaded D2EHPA. The presence of water thus strongly alters the structure of the aggregate.[20,52]

Neuman and Ibrahim probed the structure of these aggregates using ^{1}H NMR spectroscopy and molecular dynamics (MD) simulations, concluding that the structure consists of $NiA_2(H_2O)_2$ units interconnected by hydrogen bonds, with water molecules occupying the voids between the hydrophobic side chains. However, the assignments in ^{1}H NMR spectra remain ambiguous, and little experimental evidence supports the existence of the proposed coordination unit. This unit was assumed to be invariable in the MD simulations, restricting the unbound water molecules to pockets near the phosphate groups in the otherwise apolar *n*-heptane continuum. Further study is thus necessary to either support or contradict these findings.

Karl Fischer titration of samples of D2EHPA and Ionquest 290 loaded with Ni(II) in 2 : 1 stoichiometry (10 wt% NiA_2) revealed the presence of approximately 9 to 10 (9.3) molecules of water per Ni(II)–D2EHPA complex and 4 to 5 (4.8) molecules of water per Ni(II)–Ionquest 290 complex. Differential scanning calorimetry (DSC) up to a temperature of 180 °C recorded an endothermic event between 100 and 120 °C in the Ni(II)–D2EHPA sample (in the high-boiling diluent Exxsol D120), while no such event was found for Ni(II)–Ionquest 290 (in Exxsol D120). DSC traces are shown in the SI, Fig. S18 and S19.

To confirm whether this event corresponds to the loss of outer-sphere water and to quantify the number of water molecules lost in this event, the D2EHPA sample was added to a solution of water (40 wt%) in 1-butyl-3-methylimidazolium bromide, [bmim][Br], an ionic liquid which is miscible with water but fully insoluble in aliphatic solvents. At 40 wt% water, the resulting water activity corresponds to a boiling point of approximately 128 °C (assuming ideality), according to the Clausius–Clapeyron relation. Thus, this solution will extract all water with a boiling point below 128 °C from the Ni(II)–D2EHPA aggregate. Karl Fischer titration after water extraction showed that 5.9 water molecules remained per Ni(II) center. Thus, it is likely that 6 water molecules reside in the inner coordination sphere in the Ni(II)–D2EHPA complex, while 3 to 4 reside in the outer sphere, solvated by D2EHPA anions. Conversely, only 4 water molecules are present in the Ni(II)–Ionquest 290 complex, all in the inner sphere (although some solvated water may be present at a concentration of less than 1 molecule per Ni(II) center).

The above findings are corroborated by UV-vis-NIR absorption spectroscopy (Fig. 3 and 4). Spectra were recorded of 10 wt% solutions of the NiA_2 complex in heptane with water added in various stoichiometric ratios (concentration verified by Karl Fisher titration). Anhydrous complexes of Ni(II) with both D2EHPA and Ionquest 290 are tetrahedral, as can be inferred from the high absorbance (partial voiding of the Laporte selection rule) and the presence of the spin-allowed $^3T_1 \rightarrow {}^3T_1'$ and $^3T_1 \rightarrow {}^3A_2$ transitions as well as the weak, sharp, spin-forbidden $^3T_1 \rightarrow {}^1E$ and $^3T_1 \rightarrow {}^1T_1$ transitions (Fig. 3a and 4a).[53] The Ni(II)–D2EHPA complex could not be fully dehydrated (0.5 eq. water remaining), and this spectrum likely represents a structure similar to that of Ni(II)–Ionquest 290 with 0.4 eq. of water present, which is tetrahedral but distinct from that at 198 ppm of water. The apparent split of the transition to the non-degenerate $^3A_2$ term indicates that these two tetrahedral structures are in equilibrium, with the lower-energy band corresponding to the anhydrous state structure. From 2 eq. of water onwards, the spectra clearly correspond to octahedral species, with weak absorbance bands corresponding to the spin-allowed $^3A_2 \rightarrow {}^3T_2$, $^3A_2 \rightarrow {}^3T_1$ and $^3A_2 \rightarrow {}^3T_1'$ transitions.[53] The $^3A_1 \rightarrow {}^3T_1$ transitions shows a progressive hypsochromic shift with increasing water content, indicating the displacement of extractant ligands from the inner sphere by water molecules. At saturation with water, the spectrum for Ni(II)–Ionquest 290 corresponds to that with 4 equivalents of added water, while that for Ni(II)–D2EHPA shifts further with respect to the spectrum with 6 equivalents of added water. The latter is likely a result of further solvation of the $[Ni(H_2O)_6]^{2+}$ coordination unit by outer-sphere water molecules, bringing the resulting spectrum closer to that of aqueous Ni(II) ions. The changes in UV-vis absorption spectra are also evident from visual inspection of the samples (see the SI, Fig. S29). When fully anhydrous, the Ni(II)–Ionquest 290 solution markedly increases in viscosity, similar to the Co(II) samples at high loading, indicating that a similar coordination polymer with tetrahedral coordination may also be present.

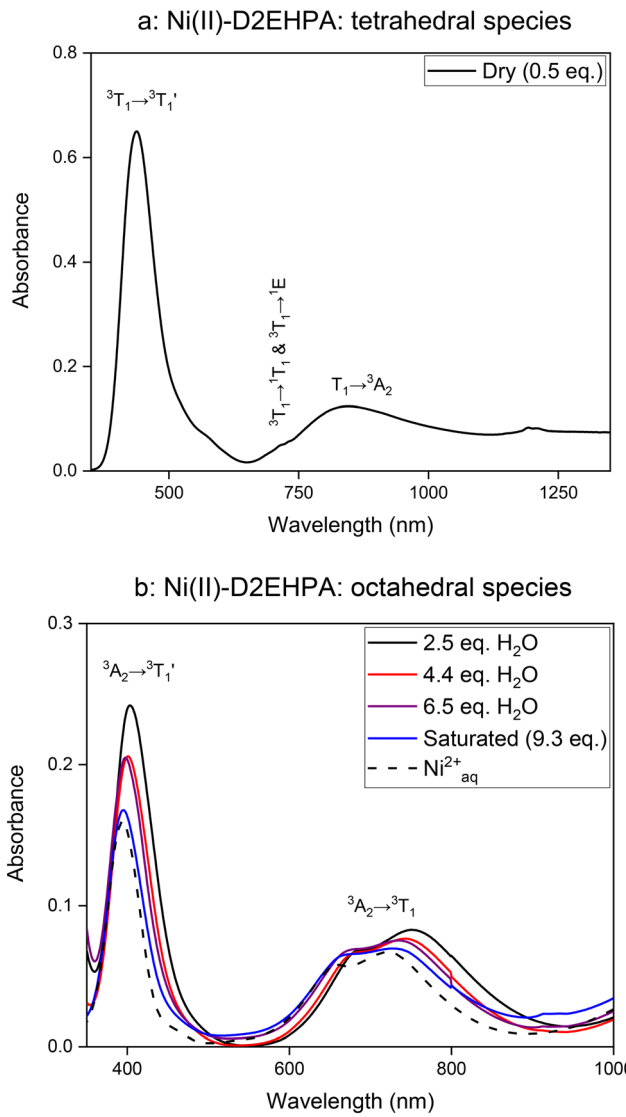

Fig. 3 UV-vis-NIR absorption spectra of D2EHPA in heptane loaded with nickel(II) (10 wt% NiA_2) at various degrees of hydration. Spectra were normalized to a path length of 2 mm.

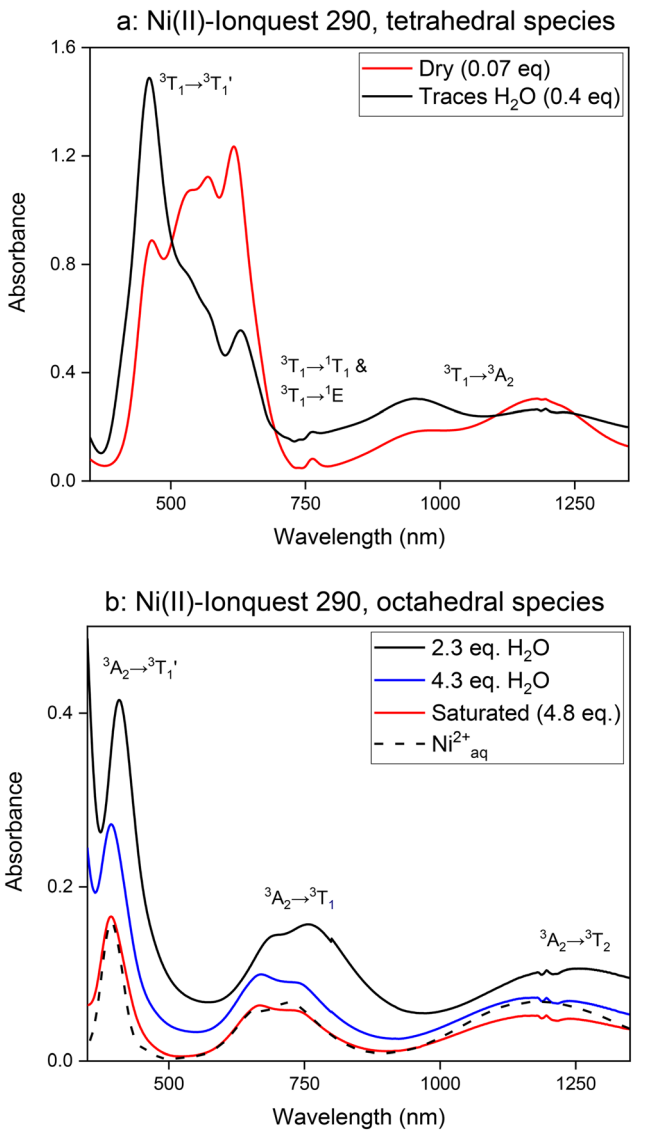

Fig. 4 UV-vis-NIR absorption spectra of Ionquest 290 in heptane loaded with nickel(II) (10 wt% NiA_2) at various degrees of hydration. Spectra were normalized to a path length of 2 mm.

^{31}P NMR studies were also carried out on the partially hydrated samples of Ni(II)–D2EHPA and Ni(II)–Ionquest 290. For the sake of brevity, a full discussion is omitted here but provided in the SI (page S23). The ^{31}P NMR spectra show the signals resulting from the phosphorus nuclei in the extractant molecules, furnishing information on the coordination mode. Spectra recorded at lower hydration (<4 equivalents of water) feature sharp, discrete signals, indicating that the ligand exchange rate is not in the regime in which extreme peak broadening occurs, and that relaxation enhancement due to paramagnetic interactions with the Ni(II) center do not excessively broaden the signal of the ^{31}P nucleus of the ligands. Nonetheless, the observed signals broaden significantly above 2 equivalents of water, particularly in the Ni(II)–D2EHPA system, and this broadening is accompanied by a visually more rapid decay of the free induction decay (FID) in the time domain, which suggests more rapid relaxation due to reduced mobility of the phosphorus nuclei. This can be interpreted as evidence of supramolecular structure formation. Thus, micellar structure formation appears to be dependent on the displacement of inner-sphere extractant anions by coordinated water molecules. At saturation with water, the chemical shift of ^{31}P in the Ni(II)–D2EHPA system is identical to that at 6 eq. of water, while samples with lower degrees of hydration exhibit significantly different chemical shifts. This further supports the notion that the inner-sphere coordination of the phosphate group changes when adding up to 6 equivalents of water, while further water is present only in the second sphere, without significantly altering the chemical shift of the phosphate group. These results can also be related to the SANS results obtained by Steytler *et al.*, who observed the formation of free, monomeric

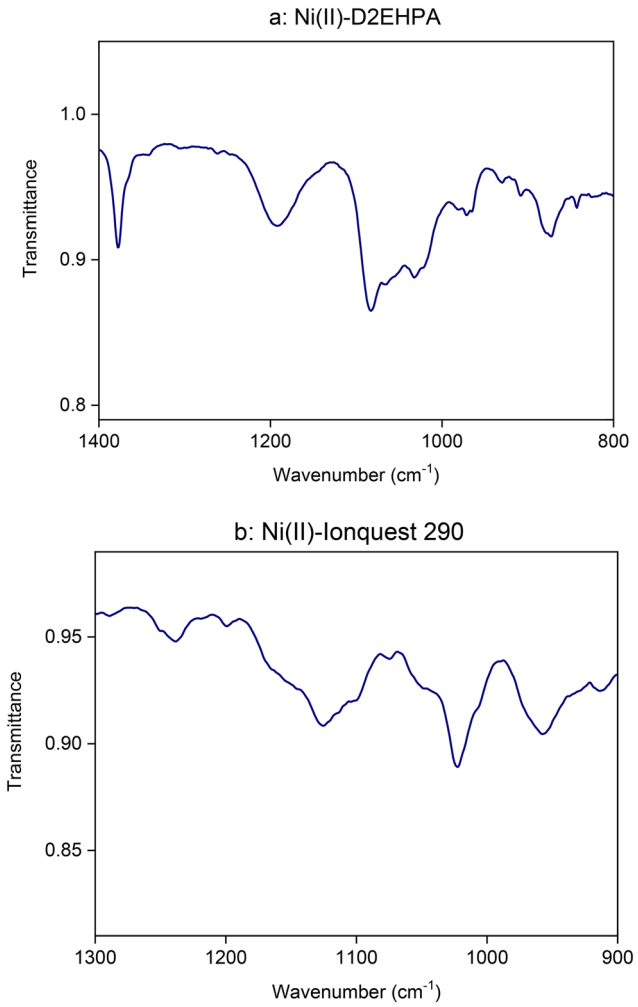

Fig. 5 FT-IR spectra of D2EHPA (10 wt% NiA_2 in heptane (a) and Ionquest 290 (30 vol% Ionquest 290 in Exxsol D120 (b) after loading with nickel(II). Peaks are listed in the SI (Table S2).

species in Ni(II)–D2EHPA at low degrees of hydration (likely the $Ni(H_2O)A_2$ complex), which polymerized into rodlike micelles upon addition of water.[54]

The FT-IR spectra of the Ni(II)-loaded organic phase at saturation with water nuance the view of an unstructured second coordination sphere. The spectrum of D2EHPA, fully loaded with Ni(II) (10 wt% NiA_2 in heptane, Fig. 5a), exhibits a single antisymmetrical phosphate stretching band at 1192 cm^{-1}, and 5 symmetrical stretching bands with peaks and shoulders at approx. 1083, 1065, 1054, 1032 and 1021 cm^{-1}. The symmetrical stretching bands are of roughly equal intensity and do not appear to exhibit any grouping. They thus likely correspond to various hydrogen bonded states for the D2EHPA A^- anion (intramolecular vibrational coupling would be expected to yield an even number of components for a NiA_2 stoichiometry, depending on the size of the primitive cell of the structure). The overall gap between the symmetrical and the antisymmetrical components is somewhat larger than that of Co(II)–D2EHPA at 100% loading, but significantly smaller than that of Co(II)–D2EHPA at 50% loading, pointing towards a moderately high local symmetry around the phosphate groups. This is consistent with A^- anions undergoing weak asymmetrical interactions with hydrogen bond donors. The barycenter of the spectrum remains at relatively low wavenumber. This indicates that the second sphere A^- anions still donate significant electron density through hydrogen bonding. The origin of the electron density is the binding LUMO (containing the delocalized π-bond), and hence its depopulation will lower the bond order in the phosphate group.

The FT-IR spectrum of the Ni(II)–Ionquest 290 system (10 wt% NiA_2 in Exxsol D120, Fig. 5b) is rather complex, exhibiting many peaks and shoulders. Analysis of the blank-subtracted spectrum and deconvolution (see the SI, Fig. S5 and S6) allowed identifying two antisymmetrical phosphinate stretching bands at 1125 and 1100 cm^{-1} and two symmetrical stretching bands at 1055 and 1023 cm^{-1}. The strong splitting of the antisymmetrical component, which was not observed for any other M(II)–Ionquest 290 complex, indicates the presence of two strongly different phosphinate environments. The bands at 1125 cm and 1023 cm^{-1} are markedly stronger than those at 1100 and 1055 cm^{-1} and thus likely constitute a pair corresponding to the same phosphinate environment. The large separation of the symmetrical and antisymmetrical components in the former pair indicates an asymmetric environment, suggesting a strong hydrogen bond with one of the oxygen atoms in the second-sphere A^- anion. The small separation of the other pair of bands implies a highly symmetrical environment, attributable to a bidentate inner-sphere A^- ligand.

The aforementioned findings demonstrate that Ni(II) binds sufficient water in its first coordination sphere to displace extractant anions to the second sphere. Accordingly, it is the weakest extracted of all 4th period divalent metal ions.[7] The Ni(II)–D2EHPA complex consists of a $[Ni(H_2O)_6]^{2+}$ unit with two second-sphere A^- anions, which can occupy one of a number of slightly different orientations in structured, cylindrical micelles which solvate 4 free water molecules per Ni(II) center (Fig. 1, type IV). Conversely, the coordination unit in the Ni(II)–Ionquest 290 system is the $NiA(H_2O)_4^+$ cation, with a single A^- anion in the second sphere with a more sharply defined orientation (Fig. 1, type V). The proposed structures elucidate why steric demands of the side chains of the extractant influence phosphinic acid extractants more strongly than phosphoric acid extractants, as none of the phosphate ligands are effectively present in the inner sphere of the Ni(II) ion.[29]

Magnesium(II)

As a 3rd period metal cation, the ionic radius of magnesium(II) is relatively small. Slope analysis with respect to the free extractant concentration was thus carried out (Fig. 6), as it is conceivable that the number of bound extractant dimers may differ for smaller ions. The slope analysis method is fully

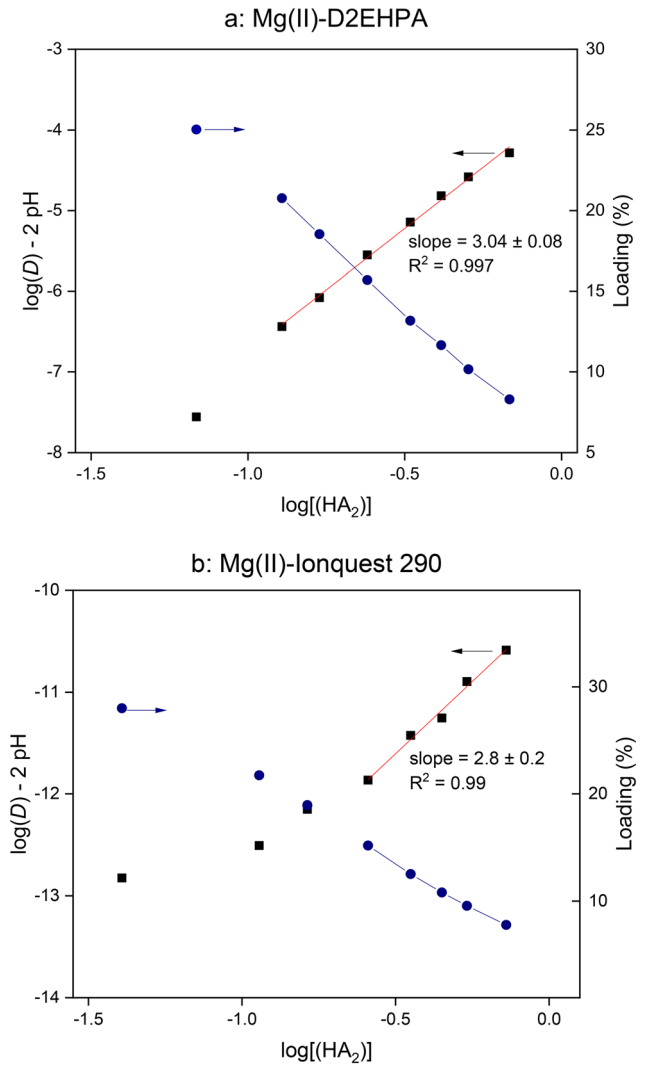

Fig. 6 Slope analysis of the extraction equilibria of magnesium(II) by D2EHPA (a) and Ionquest 290 (b) in heptane at low loading (22 °C, 150 mM $MgCl_2$, phase volume ratio = 1 : 1). Data points outside the linear interval are omitted from the regression.

elaborated in the SI (page S6). In these assays, the equilibrium concentration of the extractant is calculated by assuming the interaction of a hypothetical q extractant dimer with the extracted metal ion. This value must be a half-integer. If the slope of the curve matches the assumed value of q, the hypothesis is considered validated. The points closest to the maximal loading for a particular value of q are omitted as they deviate from the linear trend due to changing speciation. For Mg(II) extraction by D2EHPA, a value of 3.0 yields excellent correspondence, with a slope of 3.04 ± 0.08. Strikingly, this implies the involvement of 3 extractant dimers $(HA)_2$ in the extraction of a single metal ion at low loading. It should be noted that this assay does not distinguish between inner and outer sphere coordination. In the Mg(II)–Ionquest 290 system, the closest matching half-integer was also a value of q = 3, affording a slope of 2.8 ± 0.2 for the data points below 20% loading. A divergence from linearity is observed above 20% loading, although a structure with q = 3 is stoichiometrically possible until a loading of 33%.

Karl Fischer titration was used to determine the number of water molecules present at saturation per Mg(II) ion at 30%, 50% and 100% loading for both D2EHPA (245 g L^{-1} in heptane) and Ionquest 290 (183 g L^{-1} in heptane). The Mg(II)–D2EHPA system was found to solvate 3–4 (3.4) molecules of water per Mg(II) center at 30% and 50% loading, but <0.5 at 100% loading. In contrast, the Mg(II)–Ionquest 290 complex did not solvate more than 0.5 molecules of water per Mg(II) center at any percentage loading, and the detected water was likely bulk water as opposed to coordinated water.

DSC revealed an exothermic event between 90 and 105 °C in the trace of the Mg(II)–D2EHPA system at 50% loading in the high-boiling diluent Exxsol D120 (see the SI, Fig. S20). After applying the water extraction technique described for Ni(II)–D2EHPA above, approximately 2 (2.1) molecules of water were found to remain per Mg(II) center using Karl

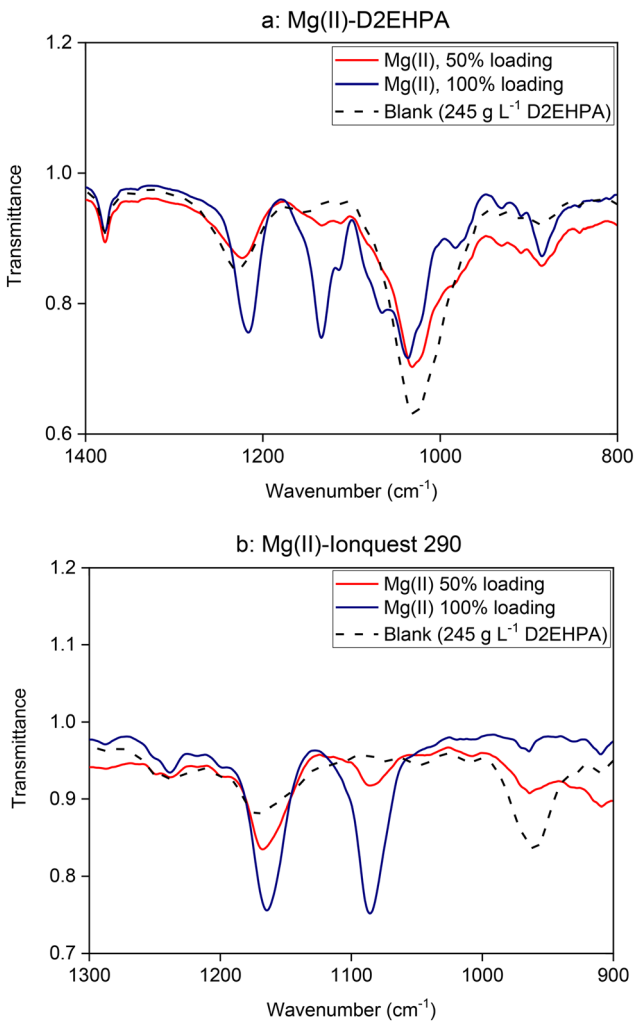

Fig. 7 FT-IR spectra of D2EHPA (245 g L^{-1} in heptane (a) and Ionquest 290 (183 g L^{-1} in heptane (b) after loading with magnesium(II). Peaks are listed in the SI (Table S3).

Fischer titration. Two of the water molecules thus appear to be bound in the first coordination sphere of the Mg(II) ion, while 1 to 2 are present in the second sphere.

The infrared spectra of the two Mg(II) systems are shown in Fig. 7. At 50% loading, the phosphate stretching band of the Mg(II)–D2EHPA system exhibits an antisymmetrical component at 1234 cm^{-1} and a symmetrical component at 1032 cm^{-1} (Fig. 7a). As with Co(II), the antisymmetrical component is shifted bathochromically, while the symmetrical component remains virtually unshifted with respect to the free $(HA)_2$ dimer. The bathochromic shift of the antisymmetrical component is, however, smaller than for Co(II), reflecting a more weakly covalent interaction between the extractant dimer and the Mg(II) ion. In addition, the local symmetry around the phosphoryloxy will accordingly be lower, and accordingly the split between the symmetrical and the antisymmetrical components is greater. Identical features

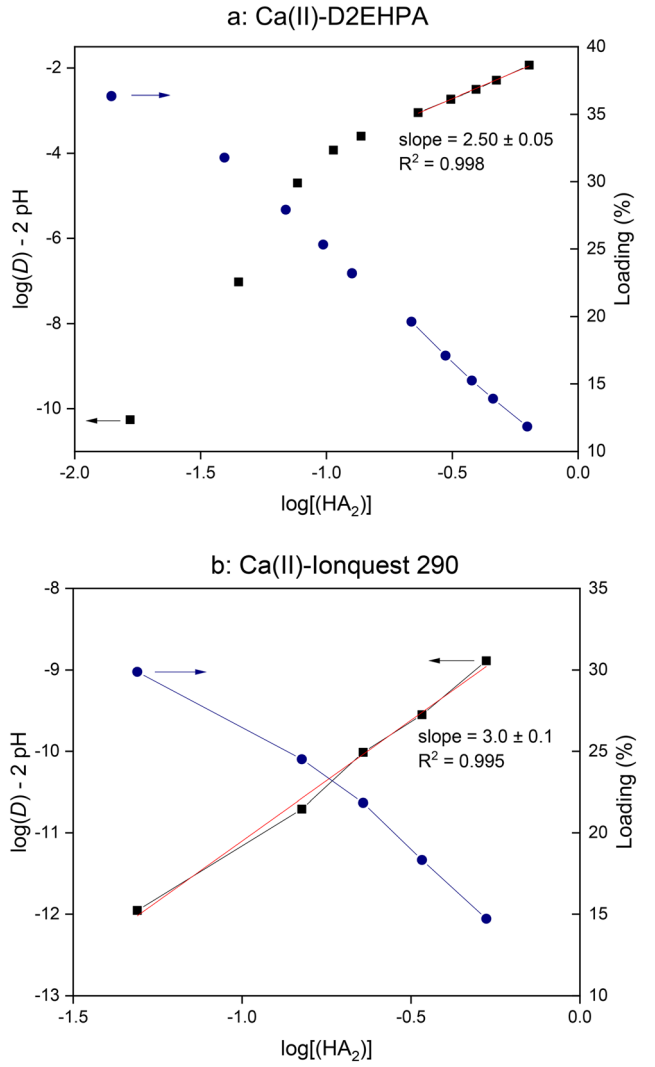

Fig. 8 Slope analysis of the extraction equilibria of calcium(II) by D2EHPA (a) and Ionquest 290 (b) in heptane at low loading (22 °C, 150 mM $CaCl_2$, phase volume ratio = 1 : 1). Data points outside the linear interval are omitted from the regression.

are seen in the spectrum at 30% loading. The absence of an additional set of phosphate bands indicates that the third $(HA)_2$ dimer involved in the binding is likely present in the second sphere, and hence largely unperturbed with respect to the free $(HA)_2$ dimer.

At 100% loading, the Mg(II)–D2EHPA system (245 g L^{-1} D2EHPA in heptane) exhibits a further reduction in the split between the symmetrical and the antisymmetrical components, as is observed in the Co(II) system (Fig. 8a). Bands are observed at 1216 cm^{-1} (antisymmetrical component) and at 1134, 1114, 1066 and 1037 cm^{-1} (symmetrical component). While the grouping of the constituent bands of the symmetrical component is not as evident as it is for the Co(II) system, the pattern is similar, and likely the result of a polymeric structure with alternating single and triple phosphate bridges linking the Mg(II) centers. The polymeric structure of the complex is supported by the high viscosity of the organic phase at 100% loading with Mg(II).

The Mg(II)–Ionquest 290 system (183 g L^{-1} Ionquest 290 in heptane) shows two sharp bands in its infrared spectrum at 100% loading, located at 1165 and 1086 cm^{-1} (Fig. 7b). The relatively small separation of these bands, respectively corresponding to the antisymmetrical and symmetrical components, reflects a high local symmetry. As the viscosity of the organic phase is very high at 100% loading, a coordination polymer with bridging Ionquest 290 anions is likely present. The barycenter of the two components is located at a strikingly high wavenumber, with the antisymmetrical component being shifted only slightly with respect to the phosphoryl group in free $(HA)_2$ dimers. This is indicative of weakly covalent Mg(II)–phosphinate bonding, with a correspondingly high electron density in the LUMO of the phosphinate group.

The infrared spectrum of the Mg(II)–Ionquest 290 system at 50% loading (Fig. 7b) is not straightforward to interpret. At first sight, the spectrum differs little from that at 100% loading. The band at 1086 cm^{-1} is weaker at 50% loading and the band at 1165 cm^{-1} is shifted to a slightly higher wavenumber (1168 cm^{-1}). At 30% loading, the same trends are observed, with a further reduction in the intensity of the band at 1086 cm^{-1} (see the SI, Fig. S8). The disappearance of the bands corresponding to free $(HA)_2$ dimers (1172 and 960 cm^{-1}) is clearly observable at 30% and 50% loading. While the antisymmetrical component of the phosphinate stretching band at low loading may overlap strongly with those of the coordination polymer and free dimers due to the limited magnitude of the bathochromic shift, there is no observable symmetrical stretching band associated with the structure at low loading. The coordination polymer already appears to begin to form at <50% loading before stoichiometric constraints necessitate a MgA_2 composition. This may be rationalized in terms of the steric limitations of the small ionic radius of Mg(II), which could destabilize any structure containing the bulky HA_2^- deprotonated dimer in the first coordination sphere. The simultaneous occurrence

of two species at low loading may account for the rapid divergence from linearity observed during the slope analysis.

Considering that Mg(II) is known to commonly adopt coordination numbers of 4 and 6, the Mg(II)–D2EHPA complex thus appears to have a $Mg(HA_2)_2(H_2O)_2$ structure at a loading below 50% (Fig. 1, type VI), solvated by two protonated D2EHPA molecules in the inner sphere at a loading below 33%, which may be involved in hydrogen bonding to the polarized inner-sphere water molecules. Approx. 1–2 water molecules are coextracted with this complex. Above 50% loading, a polymeric structure forms with alternating single and triple phosphate bridges, similar to the Co(II)–D2EHPA system at high loading (Fig. 1, type III). The structure of the Mg(II)–Ionquest 290 complex is polymeric at high loading and likely similar to that of Co(II)–Ionquest 290 at high loading (Fig. 1, type II). This structure also appears to comprise a fraction of the extracted Mg(II) at lower loading as well, alongside another structure that remains elusive, but contains no structural water molecules. The closed-shell d^0 electronic structure of the Mg(II) ion precludes UV-vis-NIR studies, while the rapid ligand exchange of closed-shell divalent cations results in the appearance of an averaged signal in NMR studies. Hence, some uncertainty remains regarding the coordination geometry of the Mg(II) ion and the coordination mode of the ligands.

Calcium(II)

As the largest member of the 4th period divalent metal ion series, calcium(II) may accommodate a larger number of extractant ligands in its inner sphere. A slope analysis was thus performed at low loading in the region where large extractant-to-metal ratios are possible (Fig. 8). The Ca(II)–D2EHPA data were fitted well by q = 2.5 with a slope of 2.50 ± 0.05 up to a loading of approximately 20%. At higher loading, pH values at equilibrium start trending sharply upwards, indicating weaker extraction due to changing speciation. For the Ca(II)–Ionquest 290 system, q = 3 afforded a slope of 3.0 ± 0.1. It must be noted that these values of q include both inner- and outer-sphere extractant molecules.

Karl Fischer titration of samples of D2EHPA (241 g L^{-1} in heptane) and Ionquest 290 (183 g L^{-1} in heptane) revealed the presence of coextracted water in all samples. In the Ca(II)–DEHPA system, the number of coextracted water molecules progressively increased from 1 (0.8) at 33% loading, over 2 (1.8) at 50% loading, to 3 (3.4) at 100% loading. DSC showed that no loss of water occurs below 180 °C at 50% loading. At 100% loading, an exothermic event occurs at 140 °C, which may be attributed to the loss of a molecule of water from the inner sphere to achieve a coordination number of 6. This implies that all water is likely present in the inner sphere and that water molecules take up vacant positions in the inner coordination sphere as fewer A^- ligands are available to coordinatively saturate the Ca(II) ion (SI, Fig. S21 and S22). In the Ca(II)–Ionquest 290 system, 3 (2.9) water molecules were found per Ca(II) center at both 20% and 40% loading, which remained bound up to 180 °C as confirmed by DSC (SI, Fig. S23). Above 40% loading, gel formation occurred in the organic phase.

Infrared spectroscopy of the Ca(II)–D2EHPA system (241 g L^{-1} in heptane, Fig. 9a) revealed that the speciation is distinctly different at 33%, 50% and 100% loading. At 33% loading, the antisymmetrical component of the phosphate stretching band is observed at 1234 cm^{-1}, after subtracting 17% of the blank D2EHPA spectrum to factor in the absorption by residual unbound D2EHPA in the sample (original spectrum shown in the SI, Fig. S9). Two components are observed in the symmetrical stretching band, presenting as an intense peak at 1030 cm^{-1} and a smaller peak at 990 cm^{-1}. This points to the presence of two distinct environments for the phosphate group, one of which is highly asymmetrical with a correspondingly wide gap between the symmetrical and the antisymmetrical bands. The latter thus likely corresponds to a monodentate, neutral D2EHPA molecule, while the

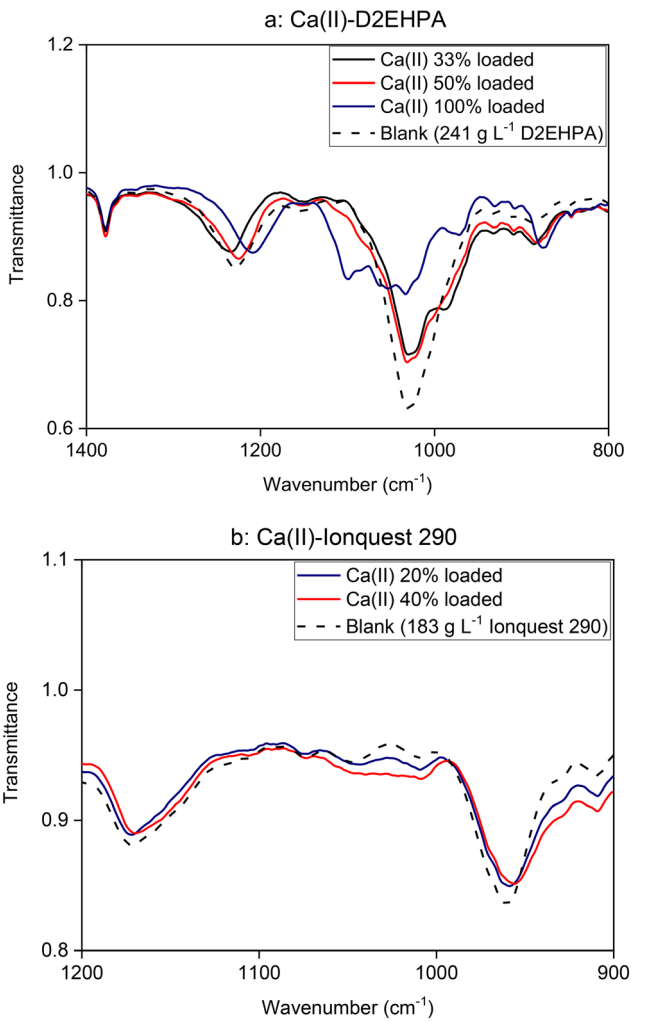

Fig. 9 FT-IR spectra of D2EHPA (241 g L^{-1} in heptane (a) and Ionquest 290 (183 g L^{-1} in heptane (b) after loading with calcium(II). Residual free D2EHPA was subtracted from the spectrum at 33% loading. Peaks are listed in the SI (Table S4).

principal band at 1031 cm^{-1} corresponds to a HA_2^- deprotonated dimer, as seen in the Co(II)–D2EHPA system at low loading (Fig. 1a). At 50% loading, the maximal stoichiometry between Ca(II) and D2EHPA is 1 : 4, precluding the inclusion of the monodentate, neutral D2EHPA molecule in the first coordination sphere. Indeed, the infrared spectrum at 50% loading no longer shows the shoulder at 991 cm^{-1}, while the other band at 1031 cm^{-1} does not shift significantly. The peak of the antisymmetrical component exhibits a modest bathochromic shift to 1125 cm^{-1}. The resulting spectrum is highly resemblant of that of the Co(II)–D2EHPA system at low loading; indicating the presence of HA_2^- dimeric ligands only.

At 100% loading, the spectrum of the Ca(II)–D2EHPA system also shows striking similarities with that of the Co(II)–D2EHPA system. A marked decrease of the gap between the symmetrical and the antisymmetrical components of the phosphate stretching band reveals an increase in local symmetry, while the splitting of the symmetrical components into two bands with disparate intensities evidences the presence of both single and triple phosphate bridges. In contrast to the Co(II)–D2EHPA spectrum, however, the band corresponding to the single bridge also appears split, which could result from the emergence of two distinct environments for the single bridge, differing in their orientation relative to the water molecules present in the Ca(II)–D2EHPA structure. The polymeric nature of this complex is supported by the high viscosity of the organic phase at 100% loading. The barycenters of the phosphate stretching regions of all Ca(II)–D2EHPA spectra are at relatively high wavenumbers, resulting from the high frequency of the antisymmetrical stretching vibration. This is indicative of a very weakly covalent Ca(II)–D2EHPA bond with limited electron transfer.

Interpretation of the Ca(II)–Ionquest 290 spectra (183 g L^{-1} in heptane, Fig. 9b) is complicated by the low intensity of the symmetrical component of the phosphinate stretching band and the strong background in the region where this band occurs. The antisymmetrical stretching band is virtually unshifted upon loading with Ca(II) up to 40%, indicating a very low degree of electron transfer from the phosphinate group to the Ca(II) ion. The blank-subtracted spectra (see the SI, Fig. S10 and S11) reveal a rise in absorbance in the 1000–1040 cm^{-1} region at 20% loading, which further increases in intensity at 40% loading. Additionally, absorbance increases in the 1040–1060 cm^{-1} region at a loading of 40%, indicating the appearance of a second phosphinate environment of higher symmetry. This could indicate the formation of bridged coordination polymers, as seen for other M(II) ions.

Ca(II) thus differs from Co(II) in the fact that its coordination sphere can accommodate higher coordination numbers, resulting in the inclusion of additional extractant molecules or water molecules in the inner sphere. At low loading, Ca(II) can accommodate 2 D2EHPA HA_2^- dimers, one neutral D2EHPA molecule and one water molecule in its inner sphere. This affords the $Ca(HA_2)_2(HA)(H_2O)$ complex (Fig. 1, type VII) While this stoichiometry is theoretically possible up to a loading of 40%, the speciation of extracted Ca(II) begins to shift prior to this point, starting around 20% loading. In the 40–50% loading range, the neutral D2EHPA molecule is replaced by a second molecule of water to yield $Ca(HA_2)_2(H_2O)_2$ (Fig. 1, type VI). Above 50% loading, polymerization of the complex occurs, with the formation of alternating single and triple phosphate bridges between the Ca(II) centers and three additional inner-sphere water ligands per Ca(II) ion (Fig. 1, type VIII). The coordination number of the Ca(II) ion in this species is 7. In Ionquest 290, Ca(II) binds to three $(HA)_2$ dimers and 3 water molecules at low loading. As the coordination number is limited to 8 for Ca(II), one of the dimers is likely present in the second sphere, possibly hydrogen bonded to the polarized inner-sphere water molecules. The coordination unit is thus likely $Ca(HA_2)_2(H_2O)_3$, with a coordination number of 7, stabilized by hydrogen bonding (Fig. 1, type IX). Above 33% loading, insufficient free Ionquest 290 is available to form this second-sphere structure, and infrared spectroscopy suggests that symmetrical (double-bridged), polymeric structures with bridging phosphinate ligands may begin forming, while retaining 3 water molecules per Ca(II) center in the first coordination sphere (Fig. 1, type X). Considerations similar to those for Mg(II) preclude further validation of these hypotheses by UV-vis-NIR or NMR spectroscopy.

Manganese(II)

The stoichiometry of Mn(II) to D2EHPA has been reported as 1 : 2.5 or 1 : 2.[16,55,56] Karl Fischer titration revealed the presence of an average of 1.7, 1.3 and 0.7 molecules of water per Mn(II) center at 30, 50 and 100% loading, respectively (245 g L^{-1} D2EHPA in heptane). DSC showed these water molecules to be present exclusively in the first coordination sphere (SI, Fig. S24). This indicates a simultaneous occurrence of hydrated and anhydrous complexes, with the former predominating at lower loading. In the Mn(II)–Ionquest 290 system (183 g L^{-1} in heptane), only trace amounts of water were detected.

Mn(II) is a d^5 ion, and as a result both tetrahedrally and octahedrally configured metal centers will exhibit the same transitions in their UV-vis-NIR absorption spectra.[57] Six spectral features can be identified in the recorded spectra for both the Mn(II)–D2EHPA and the Mn(II)–Ionquest 290 systems (245 g L^{-1} D2EHPA or 183 g L^{-1} Ionquest 290 in heptane, Fig. 10a and b, respectively), which can be assigned using the appropriate Tanabe–Sugano diagram.[53] The $^6A_1 \rightarrow {}^4T_2$ and $^6A_1 \rightarrow {}^4T_1$ transitions are visible as two poorly resolved bands near 500 nm. Around 400 nm, the $^6A_1 \rightarrow {}^4A_1$ and $^6A_1 \rightarrow {}^4E$ transitions occur as two well-resolved but weak lines. The narrow nature of these features corroborates their assignment to transitions that do not involve a change in configuration, as this renders them unaffected by line broadening due to the vibrationally oscillating crystal field strength (*i.e.* vibronic coupling).[53] In the spectrum for

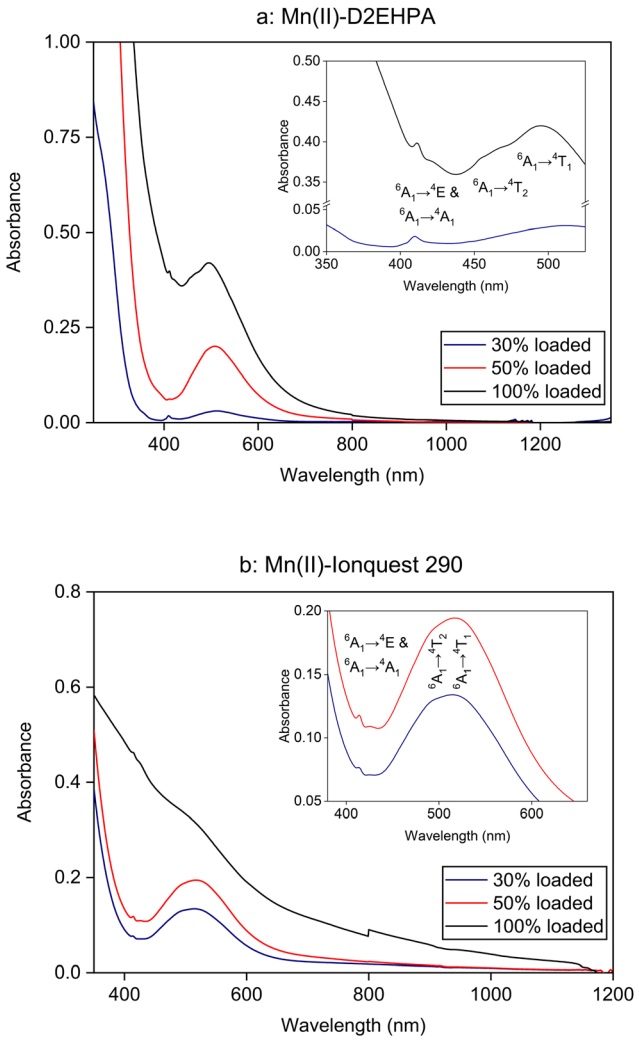

Fig. 10 UV-vis-NIR absorption spectra of D2EHPA (a, 245 g L^{-1} in heptane) and Ionquest 290 (b, 183 gL^{-1} in heptane) loaded with manganese(II) at various percentage loadings. Spectra were recorded at a path length of 2 mm.

Mn(II)–D2EHPA at 30% loading, the second $^6A_1 \rightarrow {}^4T_2$ transition is visible as a shoulder of the highly intense charge transfer band, which occurs below 400 nm. With the exception of the charge transfer band, all transitions are both spin and Laporte forbidden.

Typical of d^5 metal ions is a high degree of configuration interaction in the weak-field limit, leading to a minimal dependence of the transition energies on the crystal field strength for weak-field ligands.[53,58] The relatively short wavelengths of the $^6A_1 \rightarrow {}^4T_2$ and $^6A_1 \rightarrow {}^4T_1$ transitions in the spectra shown in Fig. 10a and b indicates that the crystal field is indeed weak in the organic phase (a stronger field strength induces a marked reduction of the energy of these transitions). The transition energies can thus not be unambiguously used to distinguish between octahedral and tetrahedral coordination. Conversely, the relative intensity of the various transitions is a good indicator for the symmetry of the complex due to relaxation of Laporte's rule under lower symmetry conditions. In a near-perfect octahedral crystal field, such as in $[Mn(H_2O)_6]^{2+}$, all transitions have similar extinction coefficients at their maximal wavelengths.[59] In tetrahedral fields, by contrast, transitions to T states may have maxima up to 25 times more intense than those to A or E states, corresponding to the transformation properties of the associated representations in the octahedral and tetrahedral point groups.[60]

At a loading of 30%, the Mn(II)–D2EHPA system has an intermediate intensity ratio between the $^6A_1 \rightarrow {}^4T_2$ and the $^6A_1 \rightarrow {}^4E$ transitions: higher than in $[Mn(H_2O)_6]^{2+}$ but lower than at 50% and 100% loading. This change indicates a significant deviation from octahedral symmetry at 30% loading, while an even greater deviation occurs at 50% and 100% loading. The intensity increase of the $^6A_1 \rightarrow {}^4T_2$ band from 50% to 100% loading is approximately twofold, indicating that the symmetry of the crystal field is likely similar in these two samples, and the increase in intensity of the band is largely due to the twofold increase in Mn(II) concentration only. In light of the above, D_{4h} symmetry seems plausible at 30% loading (axially distorted octahedral), with tetrahedral symmetry occurring at higher loading. Alternatively, the spectrum at 30% loading may be a superposition of the spectra of a weakly absorbing species of octahedral symmetry, and a low concentration of a tetrahedral species. In the Mn(II)–Ionquest 290 spectra, the ratio between the transitions to A/E and T states is high even at very low loading, indicating tetrahedral symmetry throughout the full loading range. At 100% loading, the charge transfer band becomes remarkably broad, extending far into the visible light range, indicating a potential change in speciation. The observed spectral features clearly impact the visual appearance of the samples (see the SI, Fig. S30 and S31).

The infrared spectra of both the Mn(II)–D2EHPA and the Mn(II)–Ionquest 290 systems (245 g L^{-1} D2EHPA or 183 g L^{-1} Ionquest 290 in heptane) share most of their features with

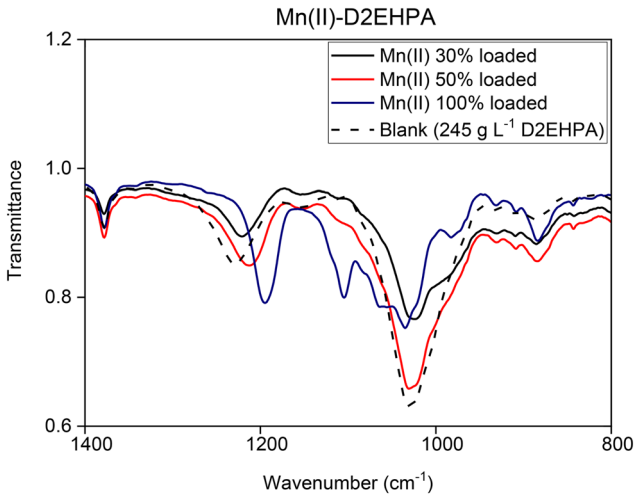

Fig. 11 FT-IR spectra of D2EHPA (245 g L^{-1} in heptane) after loading with manganese(II). Residual free D2EHPA was subtracted from the spectrum at 30% loading (Fig. S12, SI). Peaks are listed in the SI (Table S5).

those of the corresponding Co(II) systems and are thus not discussed in detail. Full spectra for Ionquest 290 are shown in the SI (Fig. S13). One point of difference exists at 30% loading in the Mn(II)–D2EHPA system (Fig. 11): in the Co(II) system, the symmetrical and antisymmetrical components of the phosphate stretching band do not shift when the loading is increased from 30% to 50%. In the Mn(II) system, however, the separation between the components is markedly larger at 30% loading due to shifts of both components. This points to the occurrence of a distinct species with a somewhat lower local symmetry around the phosphate group. The spectrum presents no evidence of D2EHPA A^- anions present in any other environment other than coordinated HA_2^- dimers.

Based on the information presented above, the structures of the Mn(II) complexes in D2EHPA and Ionquest 290 are likely very similar to those of the corresponding Co(II) species except at low loading in D2EHPA. The complex formed under these conditions is likely of D_{4h} symmetry, consisting of two axial *aqua* ligands, and two bidentate HA_2^- ligands occupying the equatorial positions (Fig. 11, type VI). At a loading of 50% in D2EHPA and at a loading of 30% and 50% in Ionquest 290, the structure is most likely tetrahedral with two HA_2^- ligands (Fig. 1, type I), although a fraction of Mn(II) may remain hydrated (octahedral) at intermediate loading in D2EHPA. At 100% loading, polymeric structures are formed, as evidenced by the high viscosity of the organic phase at high loading. The Mn(II)–D2EHPA polymer has the structure of the corresponding Co(II) polymer, with alternating single and triple phosphate bridges (Fig. 1, type III), while the Mn(II)–Ionquest 290 polymer most probably has a structure with double phosphinate bridges between every pair of adjacent metal ions (Fig. 1, type II).

The two axial water ligands in the complex formed by Mn(II) and D2EHPA at low loading may be stabilized by hydrogen-bonded interactions with free D2EHPA molecules, which exist at loading below 50%. In the absence of free D2EHPA molecules, the strong dipole of these polarized ligands remains unstabilized by the apolar diluent, promoting the release of these ligands to the aqueous phase. The smaller ionic radius of Co(II) and its resulting inability to accommodate extra ligands in the $Co(HA_2)_2$ unit could clarify why such behavior is not observed in the Co(II)–D2EHPA system.

Copper(II)

The stoichiometry of the Cu(II) complex with both D2EHPA and Cyanex 272 dimers has been reported to be 1 : 2 at low loading.[17,19] At higher degrees of loading, oligomeric species have been described by earlier authors. The relatively low degree of polymerization for Cu(II) at high loading was inferred on the basis of DLS measurements and the evolution of the distribution ratio as a function of the Cu(II) concentration.[20,24] This is reflected in the absence of a sharp increase in viscosity at high loading. Furthermore, Steytler *et al.* also found that large, linear polymeric structures can only be observed in solution in anhydrous conditions, breaking down upon addition of water.[54]

Karl Fischer titration revealed the presence of approximately 2 water molecules per Cu(II) center in the Cu(II)–D2EHPA system (245 g L^{-1} in heptane) at 30%, 50% and 100% loading (respectively 2.4, 1.8 and 1.4). Stoichiometric amounts of water were not detected in the Cu(II)–Ionquest 290 system (183 g L^{-1} in heptane), but the presence of 2 molecules of water could be inferred from the spectroscopic properties of these solutions (*vide infra*). This water could not be removed thermally without decomposition of the extractant, indicating that the failure to detect this water titrimetrically may be due to its strong binding to the Cu(II) center. DSC showed that no outer-sphere water was present in any of the samples (SI, Fig. S25).

The UV-vis-NIR absorption spectra of the Cu(II) samples exhibit only one band corresponding to a d–d transition in addition to a strong charge transfer band. This is typical for

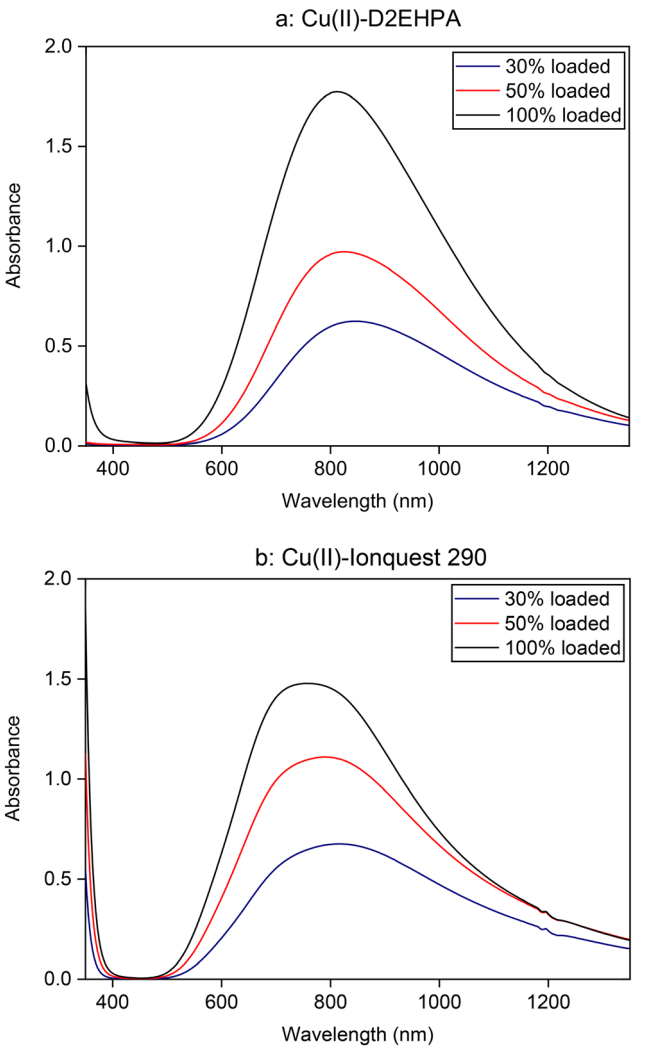

Fig. 12 UV-vis-NIR absorption spectra of D2EHPA (a, 245 g L^{-1} in heptane) and Ionquest 290 (b, 183 g L^{-1} in heptane) loaded with copper(II) at various percentages loading. Spectra were recorded at a path length of 2 mm.

d^9 ions in tetrahedral or octahedral crystal fields (Fig. 12a and b). Square planar coordination can therefore be ruled out, as this would give rise to several distinct d–d bands in the spectrum.[61] The maximum of the d–d band is located in the near infrared, around 800 nm in each sample. This suggests octahedral coordination, as tetrahedral Cu(II) species tend to absorb deeper in the infrared region, with no absorption of red light. The observed d–d band would thus correspond to the $^2A \rightarrow {}^2T_2$ transition, split into two unresolved components by the Jahn–Teller effect.[9] This split occurs due to complex, lowering the overall symmetry around the Cu(II) ion and splitting the energies of d-orbitals which are degenerate in an octahedral complex. Considering the coordination modes observed for the extractant thus far, octahedral coordination suggests the inclusion of two *aqua* ligands in the first coordination sphere, as only 2 $(HA)_2$ dimers are involved in the gross extraction mechanism.

The infrared spectra of the Cu(II)–D2EHPA (245 g L^{-1} in heptane) and Cu(II)–Ionquest 290 (183 g L^{-1} in heptane) systems are generally similar to those of Co(II). One notable exception is that of the Cu(II)–D2EHPA at 100% loading (Fig. 13). Here, the antisymmetrical phosphate stretching band is split into a component at 1222 cm^{-1} and one at 1182 cm^{-1}. The symmetrical stretching band exhibits complex splitting with numerous maxima and shoulders. This further splitting of the pattern shown by Co(II) is indicative of the presence of two distinct sets of bridging D2EHPA A^- anions, of which one has a spectral barycenter at higher wavenumber than the other. This hypsochromic shift of the barycenter is indicative of reduced electron transfer from the ligand to the Cu(II) center. The band at higher wavenumber may thus correspond to axially bound A^- anions, while equatorially bound anions vibrate at lower frequency. The Cu(II)–Ionquest 290 spectra show a bathochromic shift of the antisymmetric phosphinate stretching band at 50% loading compared to the spectrum at 30% loading. This shift can be accounted for by summing and normalizing the spectra at 30% and 100% loading (see the SI, Fig. S15), indicating that a mixture of mononuclear and oligomeric complexes may already occur at intermediate loading.

Taken together, spectral and stoichiometric data suggest the occurrence of octahedrally coordinated Cu(II) centers in the Cu(II)–D2EHPA and Cu(II)–Ionquest 290 systems, with two *aqua* ligands per Cu(II) ion. At low loading (<50%), complexes with dimeric extractant ligands of the type $Cu(HA_2)_2(H_2O)_2$ occur, with the extractant ligands likely occupying the equatorial positions (Fig. 1, type VI). At a loading above 100%, oligomeric species form with bridging extractant ligands. In the Cu(II)–D2EHPA system, these oligomers likely feature alternating tiple and single phosphate bridges between two adjacent Cu(II) ions, with phosphate groups in both equatorial and axial positions (Fig. 1, type XI). In the Cu(II)–Ionquest 290 system, in contrast, only equatorial phosphinate ligands are observed, which excludes structure type XI as a possibility and supports the presence of two bridging phosphinate groups between each pair of adjacent Cu(II) centers (Fig. 1, type XII).

Zinc(II)

On the basis of slope analysis, Zn(II) is reported to form a complex of type $ZnA(HA_2)$ after extraction by D2EHPA in aliphatic diluents, whereas extraction by Cyanex 272 yields a complex of type $Zn(HA_2)_2$.[62,63] In aromatic or other more polar diluents, a $Zn(HA_2)_2$ stoichiometry is reported for D2EHPA as well.[62] Karl Fischer titration revealed only trace amounts of water in the organic phase, implying that water is not systematically coextracted with Zn(II) in either system

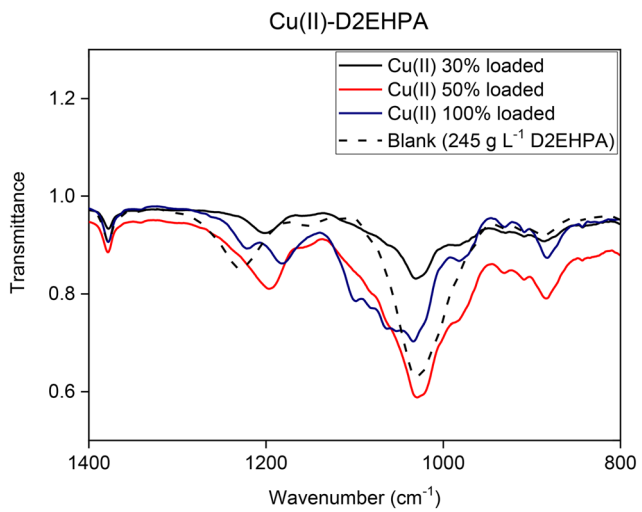

Fig. 13 FT-IR spectra of D2EHPA (245 g L^{-1} in heptane) after loading with copper(II). Residual free D2EHPA was subtracted from the spectrum at 30% loading (Fig. S14, SI). Peaks are listed in the SI (Table S6).

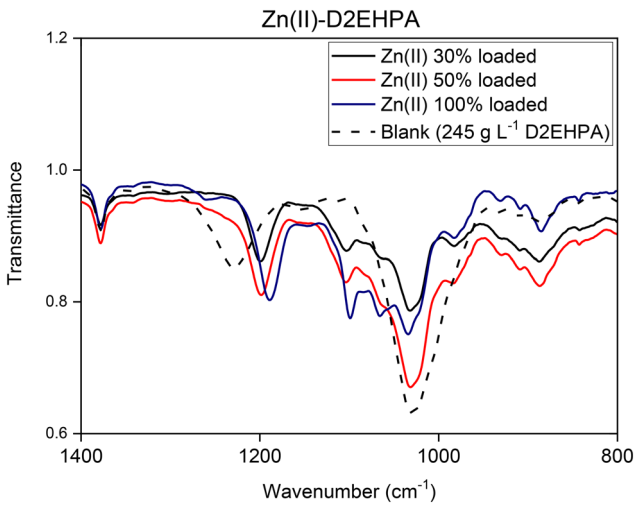

Fig. 14 FT-IR spectra of D2EHPA (245 g L^{-1} in heptane) after loading with zinc(II). Residual free D2EHPA was subtracted from the spectrum at 30% loading (Fig. S16, SI). Peaks are listed in the SI (Table S7).

(245 g L^{-1} D2EHPA or 183 g L^{-1} Ionquest 290 in heptane). Distribution ratios of Zn(II) and viscosities of the organic phase rise sharply towards very high loading as a function of the aqueous Zn(II) concentration, which is indicative of coordination polymer formation.[24]

Infrared spectroscopy appears to corroborate the presence of discrete $ZnA(HA_2)$ coordination units at low loading in the Zn(II)–D2EHPA system (Fig. 14). At a loading of 50%, the antisymmetrical component is found at 1199 cm^{-1}, whilst the main band of the symmetrical component is located at 1032 cm^{-1}. This supports a metal-bound HA_2^- dimer on the grounds of a bathochromic shift of the barycenter with respect to the free $(HA)_2$ dimer, and an intermediate symmetrical–antisymmetrical band gap. In addition, a weaker band is found at 1104 cm^{-1}, which is assigned to a distinct symmetrical phosphate stretching vibration without a resolved corresponding antisymmetrical component. The gap between the two components is thus narrow, implying a highly symmetrical local environment around this phosphate group. This is in agreement with the postulated inner-sphere A^- ligand. At a loading of 100%, the spectrum supports the exclusive presence of asymmetric polymers with bridging phosphate groups (Fig. 1, type II), as evidenced by the small gap between the symmetrical and the antisymmetrical components of the phosphate stretching vibration, and the splitting of the symmetrical component into a group of one single peak (1099 cm^{-1}) plus a group of two peaks (1066 and 1034 cm^{-1}) and a shoulder (1057 cm^{-1}). The high viscosity of the fully loaded organic phase further supports the polymeric nature of this species. The infrared spectra of the Zn(II)–Ionquest 290 system are given in the SI (Fig. S17). Their interpretation is analogous to those of the Co(II)–Ionquest 290 system, supporting the presence of the same species.

An extensive study of the Zn–D2EHPA system was also carried out by Pereira and coworkers, focusing on fitting of equilibrium data, DFT calculations and infrared spectroscopy. Fitting of experimental distribution ratios to equilibrium equations showed that, indeed, a second species with stoichiometry ZnA_2 appears in the organic phase beyond a loading of approximately 60% to 70%, in line with expectations based on stoichiometric requirements. DFT calculations indicated that a free ZnA_2 species is unstable towards association into a bridged Zn_2A_4 structure. The predicted infrared spectrum of Zn_2A_4 shows some qualitative similarity to the spectrum obtained in this work for intermediate loading. The predicted spectrum of $ZnA(HA_2)$, however, does not match any experimentally obtained spectrum, aside from the appearance of a band near 1100 cm^{-1}. The authors did not report the spectrum for full loading, shown in Fig. 14, at which point polymerization is extensive.

Thus, both stoichiometric analysis and infrared spectroscopy indicate that Zn(II) forms a unique, asymmetrical coordination unit at low loading in D2EHPA, with one bidentate HA_2^- dimer and one bidentate A^- anion in the first coordination sphere (Fig. 1, structure type XIII). At higher loading, coordination polymers with alternating single and triple phosphate bridges occur (Fig. 1, structure type III). The behavior of the Zn(II)–Ionquest 290 system follows that of Co(II)–Ionquest 290, with $Zn(HA_2)_2$ tetrahedra forming at low loading, and symmetrical polymers with double phosphinate bridges between adjacent metal centra forming at higher loading (Fig. 1, structure types I and II, respectively). The d^{10} structure of Zn(II) prevents confirmation of the proposed structures by UV-vis-NIR and NMR spectroscopy, for reasons outlined above for Mg(II).

Table 1 Summary of the structures assigned to the investigated metal ions in D2EHPA and Ionquest 290 at various percentage loadings

Metal	Loading	D2EHPA	Ionquest 290
Co(II)	30	Type I	Type I
	50	Type I	Type I
	100	Type III	Type II
Ni(II)	100	Type IV	Type V
Mg(II)	30	Type VI	n.d.[a]
	50	Type VI	n.d.[a]
	100	Type III	Type II
Ca(II)	30	Type VII	Type IX
	50	Type VI	Unstable[b]
	100	Type VIII	Unstable[b]
Mn(II)	30	Type VI	Type I
	50	Type I + type VI	Type I
	100	Type III	Type II
Cu(II)	30	Type VI	Type VI
	50	Type VI	Type VI
	100	Type XI	Type XII
Zn(II)	30	Type XIII	Type I
	50	Type XIII	Type I
	100	Type III	Type II

[a] Not determined. [b] Gel formation.

Conclusion

The mechanism of extraction of divalent metal ions by phosphorus acid extractants is more complex than often assumed, with a wide array of structures being found in the organic phase, depending on the nature of the metal ion, the extractant, and the percentage loading. Ionic radius, crystal field effects, steric demands of the extractant and the Jahn–Teller effect are all observed to affect the structure of the complex. Remarkably, extraction of Ni(II) by D2EHPA and Ionquest 290 gives rise to the formation of micellar structures in the organic phase, with second-sphere solvated extractant anions and water molecules. Nonetheless, these structures are highly regular and ordered. All other studied metal ions assemble into semi-covalent coordination polymers at high loading, leading to a viscosity increase of the loaded organic phase. An overview of the assigned structures is given in Table 1. The observed structural diversity or the metal–extractant complex cannot be ignored when describing the selectivity of extractants for various metal ions. Furthermore, this diversity warrants modifications to descriptive thermodynamic frameworks used in the modeling of solvent extraction equilibria,

particularly in modeling differences in selectivity at various degrees of loading of the extractant. A follow-up publication will focus on the elucidation of selectivity sequences in light of the results of this work.

Conflicts of interest

There are no conflicts to declare.

Data availability

The data supporting this article have been included as part of the supplementary information (SI).

Supplementary information: details on slope analysis, additional FT-IR spectra, infrared peak lists, DSC traces, ^{31}P NMR spectra and supporting photographs. See DOI: https://doi.org/10.1039/d6re00061d.

Acknowledgements

This work was funded by the European Union (ERC, CIRMET, project number 101093943). The views and opinions expressed are, however, those of the authors only and do not necessarily reflect those of the European Union or the European Research Council Executive Agency. Neither the European Union nor the granting authority can be held responsible for them. NMR spectroscopy was supported by the Research Foundation Flanders (FWO) *via* infrastructure grant I002720N. The authors would further like to extend their gratitude to Dr. Gert Steurs for technical assistance with NMR measurements.

References

1 M. Cox, in *Solvent Extraction Principles and Practice, Revised and Expanded*, ed. J. Rydberg, CRC Press, Boca Raton, 2nd edn, 2004.
2 F. Giusti, E. Guerinoni, D. Lemire, M. Thimotée, G. Arrachart, S. Dourdain and S. Pellet-Rostaing, *C. R. Chim.*, 2024, **27**, 153–183.
3 K. C. Sole, A. M. Feather and P. M. Cole, *Hydrometallurgy*, 2005, **78**, 52–78.
4 N. Krishnamurthy and C. K. Gupta, *Extractive Metallurgy of Rare Earths*, CRC Press, Boca Raton, 2004.
5 Q. Zheng, L. Zeng, Z. Cao, S. Wu, Q. Li, M. Wang, W. Guan and G. Zhang, *Green Chem.*, 2023, **25**, 10020–10032.
6 N. Peeters, K. Binnemans and S. Riaño, *Green Chem.*, 2022, **24**, 2839–2852.
7 K. C. Sole, in *Solvent Extraction and Liquid Membranes*, CRC Press, Boca Raton, 2008.
8 H. Irving and R. J. P. Williams, *J. Chem. Soc.*, 1953, 3192–3210.
9 P. Atkins, T. Overton, J. Rourke, M. Weller and F. Armstrong, *Shriver and Atkins' Inorganic Chemistry*, Oxford University Press, Oxford, 2010.
10 R. K. Biswas, M. A. Habib and M. N. Islam, *Ind. Eng. Chem. Res.*, 2000, **39**, 155–160.
11 R. K. Biswas, R. A. Banu and M. N. Islam, *Hydrometallurgy*, 2003, **69**, 157–168.
12 R. K. Biswas, M. A. Habib and H. P. Singha, *Hydrometallurgy*, 2005, **76**, 97–104.
13 I. Komasawa, T. Otake and Y. Ogawa, *J. Chem. Eng. Jpn.*, 1984, **17**, 410–417.
14 M. F. Islam and R. K. Biswas, *J. Inorg. Nucl. Chem.*, 1981, **43**, 1929–1933.
15 C. I. Sainz-Diaz, H. Klocker, R. Marr and H.-J. Bart, *Hydrometallurgy*, 1996, **42**, 1–11.
16 C. Zhang, W. Cao, J. Zhan, F. Ding and J.-Y. Hwang, *JOM*, 2015, **67**, 1110–1113.
17 K. C. Sole and J. B. Hiskey, *Hydrometallurgy*, 1995, **37**, 129–147.
18 B. K. Tait, *Hydrometallurgy*, 1993, **32**, 365–372.
19 R. S. Juang and Y. T. Chang, *Ind. Eng. Chem. Res.*, 1993, **31**, 207–213.
20 Z.-J. Yu, T. H. Ibrahim and R. D. Neuman, *Solvent Extr. Ion Exch.*, 1998, **16**, 1437–1463.
21 C. F. Baes Jr., R. A. Zingaro and C. F. Coleman, *J. Phys. Chem.*, 1958, **62**, 129–136.
22 M. L. Brisk and W. J. McManamey, *J. Appl. Chem.*, 1969, **19**, 103–108.
23 R. D. Neuman and J. P. Sang, *J. Colloid Interface Sci.*, 1992, **152**, 41–53.
24 Z. Kolařík and R. Grimm, *J. Inorg. Nucl. Chem.*, 1976, **38**, 1721–1727.
25 I. Carson, P. A. Tasker, J. B. Love, M. Moser, A. J. Fischmann, B. Jakovljevic, M. D. Soderstrom and C. A. Morrison, *Eur. J. Inorg. Chem.*, 2018, **2018**, 1511–1521.
26 I. Komasawa, T. Otake and Y. Ogawa, *J. Chem. Eng. Jpn.*, 1984, **17**, 410–417.
27 R. D. Neuman, Z.-J. Yu and T. H. Ibrahim, in *Value Adding Through Solvent Extraction - Proceedings of ISEC '96*, The University of Melbourne, Melbourne, Australia, 1996, vol. 1, pp. 135–140.
28 C. Yuan, Q. Xu, S. Yuan, H. Long, D. Shen, Y. Jiang, H. Feng, F. Wu and W. Chen, *Solvent Extr. Ion Exch.*, 1988, **6**, 393–416.
29 P. R. Danesi, L. Reichley-Yinger, G. Mason, L. Kaplan, E. P. Horwltz and H. Diamond, *Solvent Extr. Ion Exch.*, 1985, **3**, 435–452.
30 J. S. Preston and A. C. Du Preez, in *Proceedings of ISEC '86*, Dechema, Frankfurt Am Main, 1986, vol. 2, pp. 83–90.
31 Z.-J. Yu, T. H. Ibrahim and R. D. Neuman, *Solvent Extr. Ion Exch.*, 1998, **16**, 1437–1463.
32 P. Thiyagarajan, H. Diamond, P. R. Danesi and E. P. Horwitz, *Inorg. Chem.*, 1987, **26**, 4209–4212.
33 S. P. Best, S. D. Kolev, J. R. P. Gabriel and R. W. Cattrall, *J. Membr. Sci.*, 2016, **497**, 377–386.
34 H. D. Gillman, *Inorg. Chem.*, 1974, **13**, 1921–1924.
35 E. Gebert, A. H. Reis, S. W. Peterson, L. I. Katzin, G. W. Mason and D. F. Peppard, *J. Inorg. Nucl. Chem.*, 1981, **43**, 1451–1464.
36 B. A. DeAngelis, R. E. Newnham and W. B. White, *Am. Mineral.*, 1972, **57**, 255–268.
37 R. S. Halford, *J. Chem. Phys.*, 1946, **14**, 8–15.

38 R. Murugavel, A. Choudhury, M. G. Walawalkar, R. Pothiraja and C. N. R. Rao, *Chem. Rev.*, 2008, **108**, 3549–3655.
39 J. J. Hermans, L. Baij, M. Koenis, K. Keune, P. D. Iedema and S. Woutersen, *Sci. Adv.*, 2019, **5**, eaaw3592.
40 K. Gholivand, N. Fallah, A. A. Ebrahimi Valmoozi, A. Gholami, M. Dusek, V. Eigner, M. Pooyan and F. Mohammadpanah, *J. Mol. Struct.*, 2020, **1202**, 127369.
41 L. González, O. Mó, M. Yáñez and J. Elguero, *J. Chem. Phys.*, 1998, **109**, 2685–2693.
42 K. W. Oliver, *PhD Thesis*, University of British Columbia, 1984.
43 M. Khrizanforov, R. Shekurov, V. Miluykov, L. Gilmanova, O. Kataeva, Z. Yamaleeva, T. Gerasimova, V. Ermolaev, A. Gubaidullin, A. Laskin and Y. Budnikova, *Dalton Trans.*, 2019, **48**, 16986–16992.
44 S. Ondrušová, J. Hynek, J. Demel, K. Lang and M. Kloda, *J. Solid State Chem.*, 2024, **337**, 124806.
45 A. B. Andreeva, K. N. Le, L. Chen, M. E. Kellman, C. H. Hendon and C. K. Brozek, *J. Am. Chem. Soc.*, 2020, **142**, 19291–19299.
46 S.-J. Liu, R. J. Staples and J. P. Fackler, *Polyhedron*, 1992, **11**, 2427–2430.
47 J.-L. Du, S. J. Rettig, R. C. Thompson and J. Trotter, *Can. J. Chem.*, 1991, **69**, 277–285.
48 T. H. Ibrahim, *Sep. Sci. Technol.*, 2011, **46**, 2157–2166.
49 R. Grimm and Z. Kolařík, *J. Inorg. Nucl. Chem.*, 1974, **36**, 189–192.
50 J. S. Preston, *Hydrometallurgy*, 1982, **9**, 115–133.
51 R. D. Neuman, N.-F. Zhou, J. Wu, M. A. Jones, A. G. Gaonkar, S. J. Park and M. L. Agrawal, *Sep. Sci. Technol.*, 1990, **25**, 1655–1674.
52 R. D. Neuman and J. P. Sang, *J. Colloid Interface Sci.*, 1992, **152**, 41–53.
53 Y. Tanabe and S. Sugano, *J. Phys. Soc. Jpn.*, 1954, **9**, 766–779.
54 D. C. Steytler, T. R. Jenta, B. H. Robinson, J. Eastoe and R. K. Heenan, *Langmuir*, 1996, **12**, 1483–1489.
55 M. F. Islam and R. K. Biswas, *J. Inorg. Nucl. Chem.*, 1981, **43**, 1929–1933.
56 R. K. Biswas, M. A. Habib and M. G. K. Mondal, *Hydrometallurgy*, 2005, **80**, 186–195.
57 W. Moffitt and C. J. Ballhausen, *Annu. Rev. Phys. Chem.*, 1956, **7**, 107–136.
58 Y. Tanabe and S. Sugano, *J. Phys. Soc. Jpn.*, 1954, **9**, 753–766.
59 C. K. Jørgensen, *Acta Chem. Scand.*, 1954, **8**, 1502–1512.
60 F. A. Cotton, D. M. L. Goodgame and M. Goodgame, *J. Am. Chem. Soc.*, 1962, **84**, 167–172.
61 V. I. Avdeev and I. I. Zakharov, *Theor. Exp. Chem.*, 1966, **2**, 451–455.
62 T. C. Huang and R. S. Juang, *Ind. Eng. Chem. Fundam.*, 1986, **25**, 752–757.
63 M. F. Bari, M. N. Begum, S. B. Jamaludin and K. Hussin, *Miner. Process. Extr. Metall.*, 2009, **118**, 227–234.